ARTICLE

PACT suppresses PKR activation through dsRNA binding and dimerization, and is a therapeutic target for triple-negative breast cancer

ADDISON A. YOUNG,[1] ISABELLE G. JUHLER,[1] JACKSON R. PIERCE,[1] HOLLY E. BOHLIN,[1] HALEY A. HARPER,[2] DAVID S. ONISHILE,[1] RENEE N. CHUA,[1] MADISON E. LIU,[1] ESTELLE N. GARDNER,[1] BENNETT D. ELZEY,[2,3] and KYLE A. COTTRELL[1,2]

[1]Department of Biochemistry, Purdue University, West Lafayette, Indiana 47907, USA
[2]Purdue Institute for Cancer Research, Purdue University, West Lafayette, Indiana 47907, USA
[3]Department of Comparative Pathobiology, Purdue University, West Lafayette, Indiana 47907, USA

ABSTRACT

Triple-negative breast cancer (TNBC), the deadliest breast cancer subtype, lacks broadly applicable targeted therapies. Induction of "viral mimicry" by activation of viral double-stranded RNA (dsRNA) sensors has potential therapeutic applications for TNBC and other cancers. Suppressors of dsRNA sensing prevent sensing of endogenous dsRNAs and resulting autoimmunity. Depletion of the suppressor of dsRNA sensing ADAR1 causes activation of dsRNA sensors and cell death in many cancer cell lines. These ADAR1-dependent cells are generally also dependent on the dsRNA-binding protein PACT, which is highly expressed and essential in many TNBC cell lines. While PACT is known as an activator of the dsRNA sensor PKR, overexpression of PACT had no effect on activation of PKR in multiple TNBC cell lines. Conversely, depletion of PACT in PACT-dependent cell lines caused robust activation of PKR and cell death, in addition to induction of integrated stress response genes and NF-κB targets. These phenotypes were entirely dependent on PKR. Rescue experiments revealed that PACT dimerization and dsRNA binding are required to suppress PKR activation. While depletion of PACT alone in ADAR1/PACT-independent cell lines had no effect on PKR activation, combined depletion of both PACT and ADAR1 in those cell lines caused robust PKR activation and cell death, supporting a partially redundant role for ADAR1 and PACT in suppression of dsRNA sensing. Taken together, these findings support a vital role for PACT in suppressing PKR activation and highlight the therapeutic potential of targeting PACT to treat TNBC.

Keywords: dsRNA; cancer; PACT; ADAR1; RBP; PKR

INTRODUCTION

Triple-negative breast cancer (TNBC) is the deadliest form of breast cancer, with high rates of recurrence and metastasis (Curigliano and Goldhirsch 2011; Bianchini et al. 2016). A major factor driving the poor patient outcomes is the lack of broadly applicable targeted therapies for TNBC (Curigliano and Goldhirsch 2011; Bianchini et al. 2016; Waks and Winer 2019). Immunotherapies, such as immune checkpoint blockade (ICB), have shown some efficacy in TNBC, but many tumors are resistant (Morad et al. 2021). Often, tumors with increased inflammation, known as immunologically "hot" (immune inflamed), are more sensitive to ICB, relative to "cold" (immune excluded) tumors (Chen and Mellman 2017). Several recent studies have shown that increasing inflammation within tumors can overcome resistance to ICB (Ishizuka et al. 2019; Jiang et al. 2019; Guirguis et al. 2023; Huang et al. 2024; Young et al. 2024). A great example of this approach is targeting the RNA editor ADAR1 to overcome resistance to ICB in mouse tumor models (Ishizuka et al. 2019).

Adenosine deaminase acting on RNA (*ADAR*, which encodes ADAR1) has been identified as an essential gene in multiple cancer cell lines—including those derived from breast, lung, and ovarian cancer (Gannon et al. 2018; Liu et al. 2019b; Kung et al. 2021). ADAR1 deaminates adenosine to inosine in double-stranded RNAs (dsRNA) in a

Corresponding author: kacottre@purdue.edu
Handling editor: Maria Carmo-Fonseca
Article is online at http://www.rnajournal.org/cgi/doi/10.1261/rna.080637.125. Freely available online through the *RNA* Open Access option.

process known as A-to-I editing (Bass and Weintraub 1988; Bass 2024; Mendoza and Beal 2024). This function of ADAR1 is essential and prevents autoimmunity. Specifically, A-to-I editing by ADAR1 prevents activation of MDA5, a dsRNA sensor, by endogenous dsRNAs (Mannion et al. 2014; Liddicoat et al. 2015; Pestal et al. 2015). There are multiple dsRNA sensors expressed in immune and nonimmune cells that detect dsRNA arising from viral infections (Rehwinkel and Gack 2020; Chen and Hur 2022; Cottrell et al. 2024a). Because these proteins bind to dsRNA by recognizing the structure of the dsRNA, and generally lack any sequence specificity, dsRNA sensors can also be activated by endogenous dsRNAs (Cottrell et al. 2024a). Several dsRNA sensors, including MDA5, RIG-I, and TLR3, activate the type-I interferon (IFN-I) pathway to promote an antiviral response, which includes expression of IFN-stimulated genes (ISG) (Matsumoto et al. 2011; Rehwinkel and Gack 2020). The dsRNA sensor protein kinase RNA-activated (PKR) instead activates the integrated stress response (ISR) by phosphorylation of eIF2α and promotes inflammation through activation of NF-kB (Gal-Ben-Ari et al. 2018; Chukwurah et al. 2021).

Since dsRNA sensors can bind to and be activated by endogenous dsRNAs, to prevent autoimmunity, their activation must be suppressed in the absence of a viral infection. Multiple proteins suppress activation of dsRNA sensors by endogenous dsRNAs (Cottrell et al. 2024a; Young et al. 2024). These "suppressors of dsRNA sensing" function through several mechanisms. For instance, ADAR1 prevents activation of two different dsRNA sensors through distinct mechanisms. Whereas ADAR1 prevents activation of MDA5 through A-to-I editing of dsRNA, ADAR1 also prevents activation of PKR through competition for dsRNA binding (Liddicoat et al. 2015; Pestal et al. 2015; Chung et al. 2018; Hu et al. 2023). The activation of dsRNA sensors and their downstream pathways, triggered by the loss of suppressors of dsRNA sensing or other perturbations, is referred to as "viral mimicry." This term reflects cell behavior similar to that elicited by viral infection, but instead the cells are responding to endogenous dsRNAs (Chen et al. 2021; Cottrell et al. 2024a). It is this viral mimicry phenotype that overcomes resistance to ICB in ADAR1 depleted tumors and serves as a strong justification for the identification of ADAR1 inhibitors to treat multiple cancers (Ishizuka et al. 2019).

While the effects of depleting ADAR1 in cancer cells have therapeutic value, not all cancer cells are dependent on ADAR1 for proliferation (Gannon et al. 2018; Liu et al. 2019b; Kung et al. 2021). We and others have observed that depletion of ADAR1 causes cell death and/or reduced proliferation and activation of dsRNA sensors in only a subset of cancer cell lines. Roughly half of TNBC lines are dependent on ADAR1 expression, based on reduced gene dependency scores from DepMap (McFarland et al. 2018; Dempster et al. 2019; Arafeh et al. 2025). In these ADAR1-dependent cell lines, depletion of ADAR1 causes cell death and activation of multiple dsRNA sensing pathways (Gannon et al. 2018; Liu et al. 2019b; Kung et al. 2021). Conversely, in ADAR1-independent cell lines, depletion of ADAR1 has no effect on cell viability, and there is no activation of dsRNA sensors. One factor driving ADAR1-dependency is elevated expression of IFN stimulated genes (ISGs) in ADAR1-dependent cell lines. The chronic IFN-I signaling in these cells leads to elevated expression of dsRNA sensors (PKR, MDA5, OAS1-3) that are ISGs (Gannon et al. 2018; Liu et al. 2019b; Kung et al. 2021). It has been proposed that the elevated expression of dsRNA sensors in these cells creates a poised state, where the cells are highly sensitive to loss of ADAR1—or potentially the loss of other suppressors of dsRNA sensing.

ADAR1 is not the only suppressor of dsRNA sensing. For example, DHX9 and STAU1 prevent PKR activation through binding to dsRNAs (Elbarbary et al. 2013; Cottrell et al. 2024b). Like ADAR1, those proteins bind dsRNA through dsRNA binding domains (dsRBD). There are 19 human proteins that contain dsRBDs and many other dsRNA binding proteins (dsRBP) that bind via other domains, in particular helicase domains. Each of these proteins is potentially competing with PKR, or perhaps MDA5, for binding to endogenous dsRNAs.

Here we provide evidence that protein activator of the interferon-induced protein kinase (PACT) functions as a suppressor of dsRNA sensing in TNBC. We show that PACT specifically suppresses PKR activation through dimerization and dsRNA binding. In addition to PKR activation and cell death, depletion of PACT causes activation of the ISR and NF-κB pathways in PACT-dependent cell lines. In PACT-independent cell lines, our data support redundancy between PACT and ADAR1 in suppression of dsRNA sensing. Together, our findings support PACT as a therapeutic target for a subset of TNBC.

RESULTS

PACT is highly expressed in TNBC and essential in many TNBC cell lines

Since ADAR1-dependent cell lines have elevated expression of PKR and other dsRNA sensors, we hypothesized that they would be sensitive to loss of other suppressors of dsRNA sensing. As such, we turned to publicly available gene dependency data from DepMap to identify dsRBPs that may function as suppressors of dsRNA sensing like ADAR1. We determined the pairwise correlation coefficients for ADAR1-dependency scores versus the dependency scores for all other genes across all cell lines for which dependency data are available in DepMap (https://depmap.org/portal). This analysis was performed for dependency scores from CRISPR-Cas9 screens (CHRONOS) and RNAi screens (DEMETER2) (McFarland

et al. 2018; Dempster et al. 2019). Among the genes with the strongest correlation with ADAR1-dependency scores was *PRKRA*, which encodes PACT (Pearson $r = 0.341$ for CHRONOS and 0.420 for DEMETER2) (Fig. 1A,B; Supplemental Fig. S1A,B). While there are many other genes with dependency scores that significantly correlate with ADAR1-dependency, including the RNA exonuclease *XRN1*, which has previously been shown to suppress activation of dsRNA sensors (Zou et al. 2024), we decided to focus our research on PACT because it, like ADAR1, contains multiple dsRNA binding domains. Additionally, PACT was the only dsRBD containing protein with gene dependency scores that strongly correlate ($r > 0.2$) with ADAR1-depedendency (Supplemental Fig. S1C).

Analysis of pairwise correlation between PACT-dependency scores and those of all other genes revealed *ADAR* as the strongest codependent gene of *PRKRA* (Fig 1C; Supplemental Fig. S1D). Looking across lineages, PACT-dependent cell lines are common in cancers arising from multiple organs (Fig. 1D; Supplemental Fig. S1E). Given our past efforts studying ADAR1 in breast cancer, the strong correlation between PACT-dependency and ADAR1-depdency scores in breast cancer cell lines (Fig. 1E; Supplemental Fig. S1F), and several breast cancer cell lines being among the most strongly dependent on PACT, we chose to focus on studying the role of PACT in breast cancer. Analysis of PACT-dependency in breast cancer subtypes revealed a strong bias toward triple-

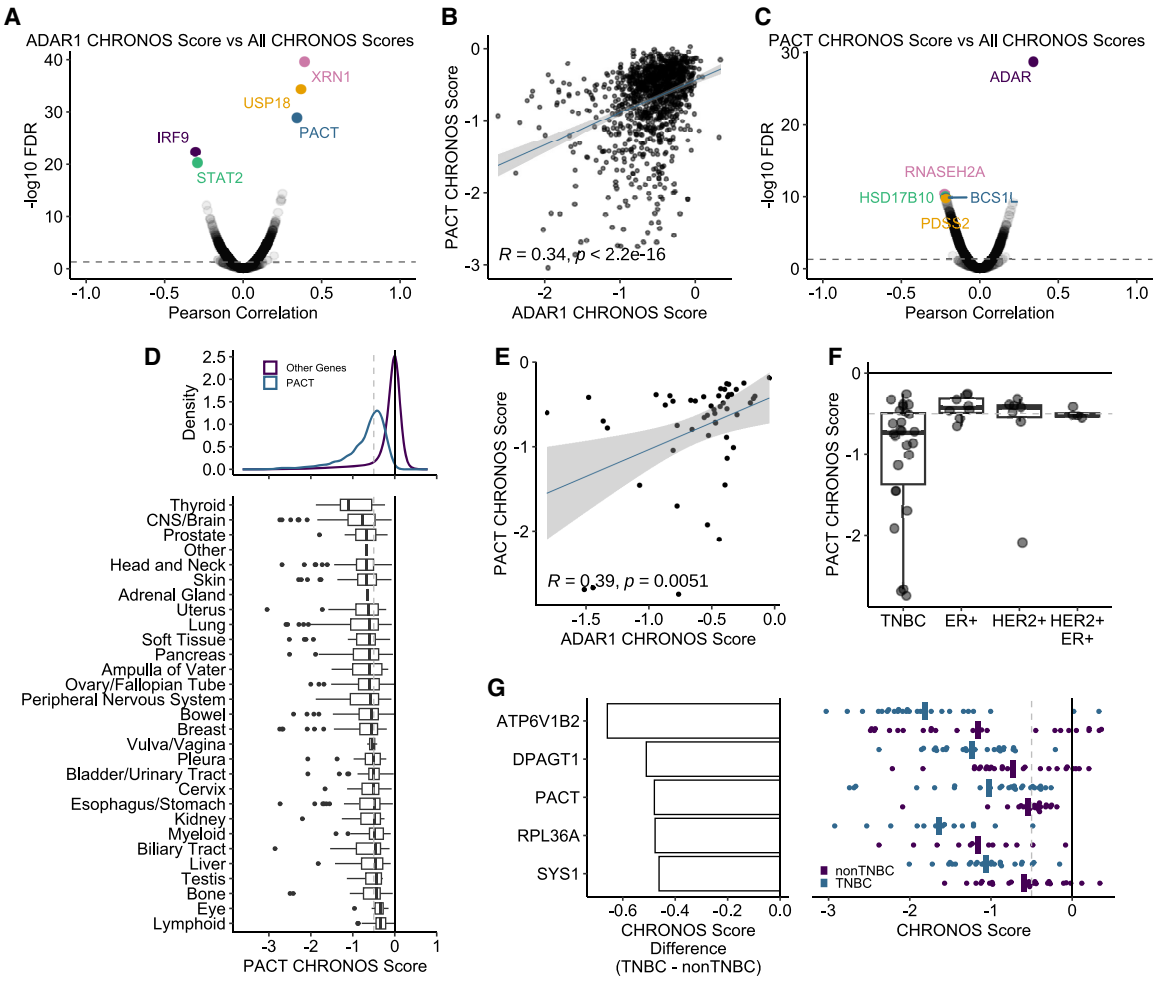

FIGURE 1. PACT is a codependency of ADAR1 and is essential in many TNBC cell lines. (*A*,*C*) Volcano plots of Pearson correlation coefficients and FDR corrected *P*-values for pairwise comparisons between ADAR1 CHRONOS score (*A*) or PACT CHRONOS score (*C*) and CHRONOS scores for all genes in DepMap across all cell lines. (*B*) Correlation between PACT and ADAR1 CHRONOS scores for all DepMap cell lines, Pearson correlation coefficient, and *P*-value are shown. (*D*, *top*) Density plot of CHRONOS scores for PACT or all other genes. (*Bottom*) Box plots for PACT CHRONOS score by lineage. (*E*) Correlation between PACT and ADAR1 CHRONOS scores for breast cancer cell lines, Pearson correlation coefficient, and *P*-value are shown. (*F*) Box plot of PACT CHRONOS scores of breast cancer cell lines separated by subtype. (*G*, *left*) CHRONOS score difference between TNBC and non-TNBC cell lines. (*Right*) CHRONOS score box plots for TNBC and non-TNBC cell lines. The top five genes based on the difference in CHRONOS scores between TNBC and non-TNBC are shown. All data are shown from DepMap.

negative breast cancer (TNBC) (Fig. 1F; Supplemental Fig. S1G–I). Interestingly, the difference between PACT-dependency scores among TNBC versus non-TNBC cell lines is larger than the difference for all but two other genes (Fig. 1G).

The expression of PACT at the RNA and protein levels varies across cell lines, with TNBC cell lines generally expressing more PACT than non-TNBC lines (Fig. 2A–C; Supplemental Fig. S2A,B). In human tumors, PACT expression is significantly elevated in TNBC relative to normal breast or other subtypes (Fig. 2D,E; Supplemental Fig. S2C,D). Elevated expression of PACT, however, is not prognostic of survival in breast cancer overall, or TNBC (Fig. 2F,G).

PACT is not an activator of PKR in TNBC

Previous research has indicated that PACT is an activator of the dsRNA sensor PKR (Patel and Sen 1998; Patel et al. 2000; Peters et al. 2001, 2009; Li et al. 2006; Singh et al. 2011; Chukwurah et al. 2021). To evaluate if PACT functions as an activator of PKR in breast cancer cell lines, we overexpressed either wild-type PACT or two phosphosite mutants of PACT (phosphomimetic S287D and

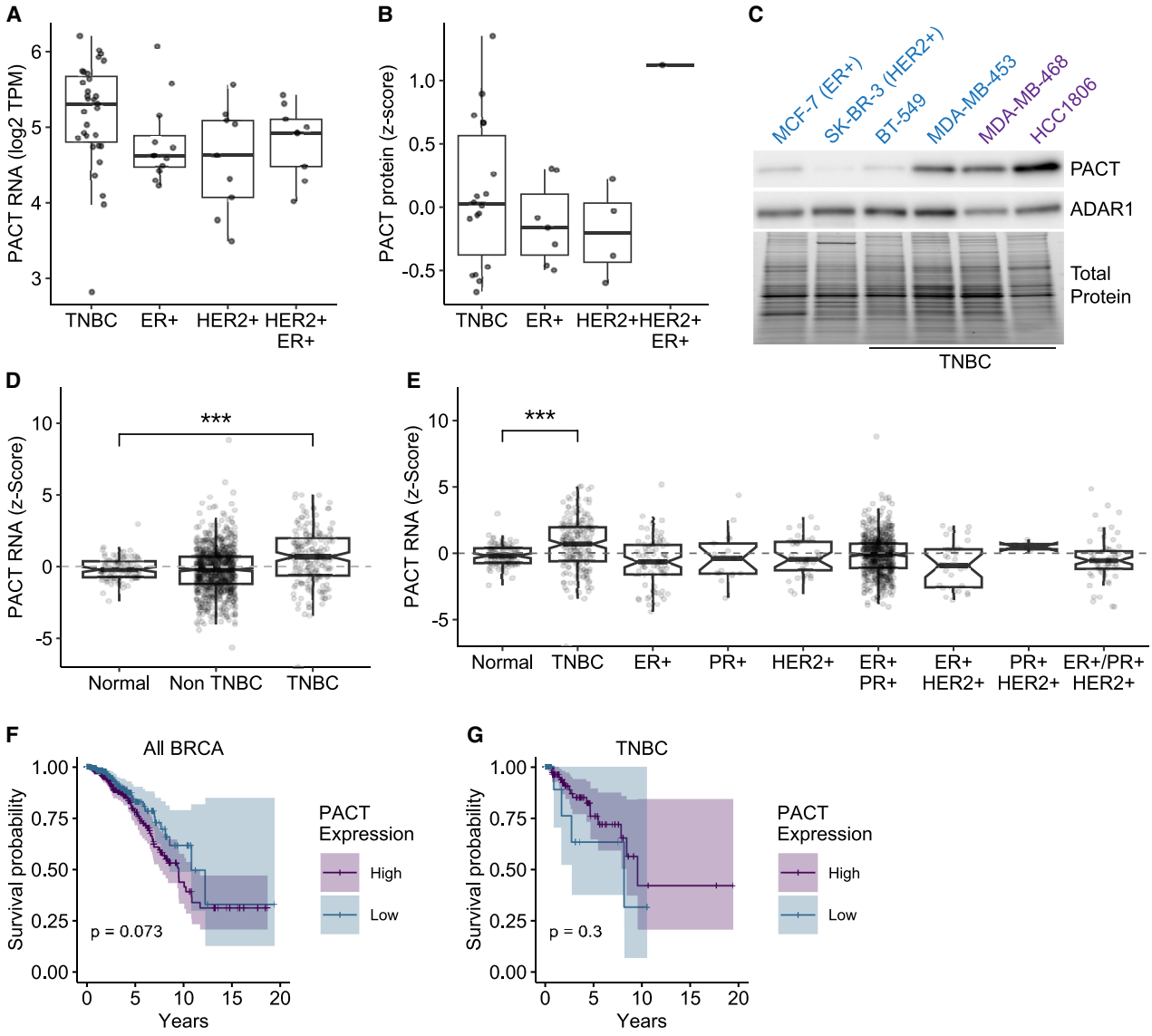

FIGURE 2. PACT is highly expressed in TNBC. Expression of PACT at the RNA (*A*) or protein level (*B*) in breast cancer cell lines separated by subtype. (*C*) Representative immunoblot for PACT and ADAR1 expression in a panel of breast cancer cell lines. Cell lines in blue are PACT-independent and purple are PACT-dependent. Total protein was imaged using a stain-free gel and serves as a loading control. (*D*,*E*) Expression of PACT at the RNA level in normal and breast tumor samples separated by subtypes. (*F*,*G*) Overall survival of breast cancer patients separated by high or low PACT expression for all tumor types (*F*) or TNBC only (*G*). For panels *A*, *B*, *D*, and *E*, data from DepMap; *F* and *G* from TCGA.

phospho-null S287A). Those mutants alter a serine residue in PACT that was previously shown to enhance activation of PKR when phosphorylated (Peters et al. 2009; Singh et al. 2011). Overexpression of neither PACT, PACT^{S287D}, nor PACT^{S287A} had any effect on PKR activation (phosphorylation of PKR on Thr-446) in four different TNBC cell lines, two PACT-dependent (HCC1806 and MDA-MB-468) and two PACT-independent (BT-549 and MDA-MB-453) (Fig. 3A,B). To further evaluate if PACT functions as an activator of PKR in cancer, we compared PACT expression at the protein level with expression of ATF4, a component of the ISR that is induced upon PKR activation (Costa-Mattioli and Walter 2020). We observed no correlation between PACT and ATF4 protein expression across cancer cell lines for which proteomic data were available (Fig. 3C). As a control, we compared ATF4 expression to ATF3, a transcription factor induced by ATF4, and found a strong correlation (Fig. 3D). Together these findings do not support PACT functioning as a PKR activator.

PACT suppresses PKR activation

To further evaluate the role of PACT in TNBC cell lines, we used CRISPR-Cas9 to deplete PACT in a panel of PACT-dependent (HCC1806 and MDA-MB-468) and PACT-independent (BT-549 and MDA-MB-453) cell lines (Fig. 4A,B). The PACT-dependent and PACT-independent cell lines chosen are also ADAR1-dependent and ADAR1-independent, respectively (Fig. 4A). Consistent with DepMap data, for PACT-dependent cell lines, depletion of PACT reduced cell viability, but in PACT-independent cell lines, depletion of PACT had no effect on viability as measured by an ATP-dependent luciferase activity (Fig. 4C). For the two PACT-dependent cell lines, we further evaluated the effect of PACT depletion on cell viability and proliferation by crystal violet staining. Depletion of PACT reduced crystal violet stained foci in both HCC1806 and MDA-MB-468 (Fig. 4D). To evaluate the in vivo effect of PACT depletion on tumorigenesis, we performed an orthotopic xenograft study with inducible knockout of PACT in HCC1806 cells. Tumorigenesis was significantly reduced by PACT depletion, highlighting the potential of targeting PACT to treat TNBC (Fig. 4E). In PACT-dependent cell lines, but not PACT-independent cell lines, depletion of PACT caused activation of PKR (Fig. 4B,F). These finding suggests that PACT functions not as an activator of PKR, but as a suppressor of PKR activation.

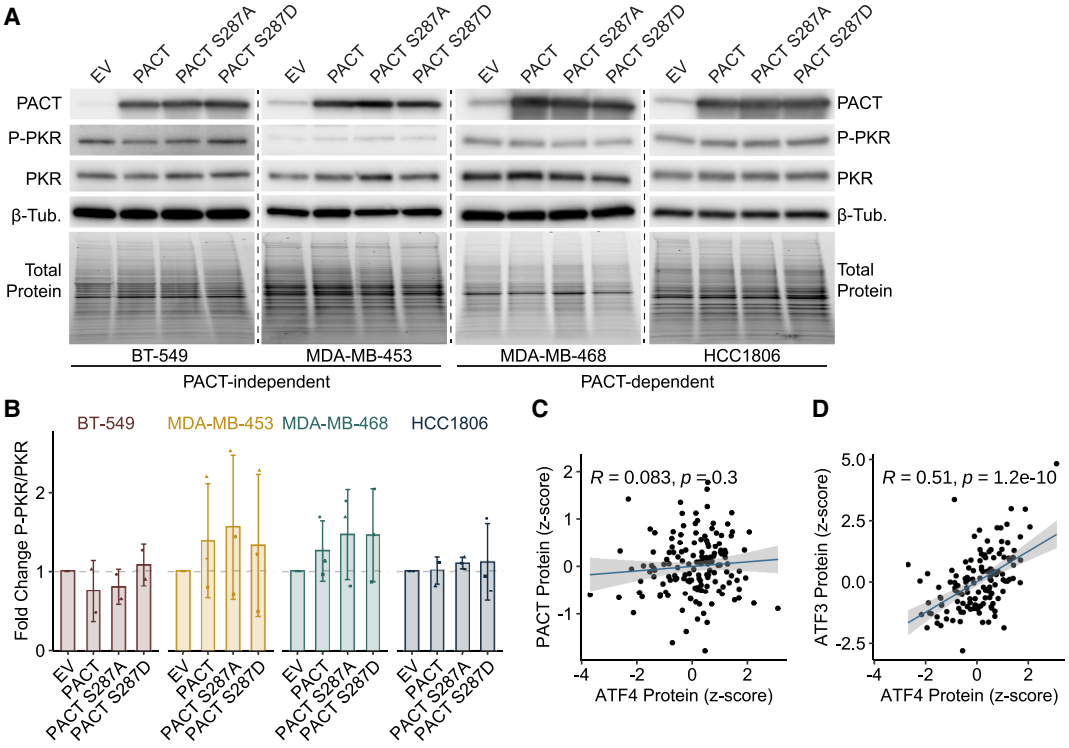

FIGURE 3. PACT overexpression does not cause PKR activation in TNBC. (*A*) Representative immunoblots for proteins of interest in control (empty vector, EV) or PACT (PACT, PACT S287A, PACT S287D) overexpressing cell lines. The blots for each cell line were performed independently and should not be compared between cell lines. Total protein was imaged using a stain-free gel and was used as the loading control for normalization. (*B*) Quantification of the blot in *A*. Bars represent the average of at least three biological replicates; error bars are ±SD. (*C*,*D*) Scatter plots comparing the protein abundance of PACT (*C*) or ATF3 (*D*) to ATF4 protein abundance across cancer cell lines, the Pearson correlation coefficient, and *P*-value are shown. Data for *C* and *D* from DepMap.

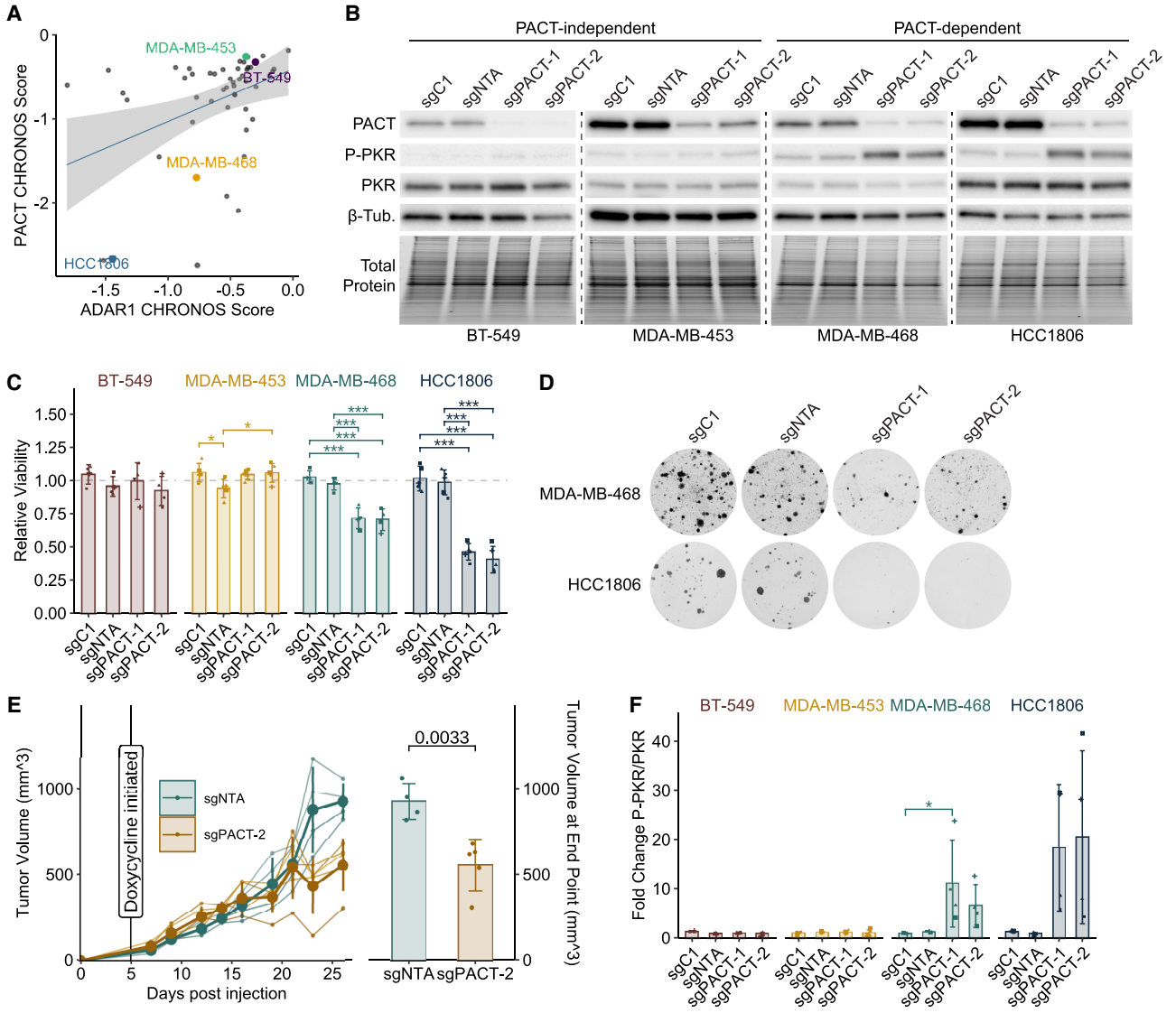

FIGURE 4. In PACT-dependent TNBC cells, PACT is required for viability, tumorigenesis, and suppression of PKR activation. (*A*) Correlation between PACT and ADAR1 CHRONOS scores of breast cancer cell lines, Pearson correlation coefficient, and *P*-value are shown; data from DepMap. The labeled cell lines are used in PACT depletion experiments. (*B*) Representative immunoblot for PACT-independent and PACT-dependent cell lines with (sgPACT-1, sgPACT-2) or without (sgNTA, sgC1) depletion of PACT. The sgNTA control is a nontargeting sgRNA, while sgC1 targets the AAVS1 locus; sgPACT-1 and sgPACT-2 are two different sgRNAs targeting PACT; see Materials and Methods for further details on all sgRNAs used. The blots for each cell line were performed independently and should not be compared between cell lines. Total protein was imaged using a stain-free gel and was used as the loading control for normalization. (*C*) Cell viability as assessed by CellTiter-Glo 2.0 in PACT depleted and control cell lines. (*D*) Representative crystal violet staining of PACT depleted and control cells. (*E*) Effect of PACT depletion on tumorigenesis of HCC1806 cells. *Left* panel is tumor volume over time, *right* panel is the final tumor volume at end point. (*F*) Quantification of the immunoblot in *B*. Bars represent the average of at least four biological replicates; error bars are ±SD. (*) $P < 0.05$, (**) $P < 0.01$, (***) $P < 0.001$. *P*-values determined by one-way ANOVA with post hoc Tukey (*C*,*F*) or *t*-test (*E*).

Activation of PKR in PACT depleted cells drives cell death and activation of ISR and NF-κB

To get a better picture of which pathways are dysregulated in PACT depleted cells, including pathways downstream from dsRNA sensors beside PKR, we performed RNA-seq on PACT depleted and control HCC1806 and MDA-MB-468 cells (both PACT-dependent) (Fig. 5A,B; Supplemental Tables S3, S4). Gene set enrichment analysis of PACT depleted HCC1806 and MDA-MB-468 identified many dysregulated pathways (Fig. 5C; Supplemental Tables S5–S8). The top two most upregulated pathways in both cell lines were associated with NF-κB signaling (Hallmark TNFA signaling via NFKB [Liberzon et al. 2015]) and the ISR (ATF4 target genes [Wong et al. 2019]). Conversely, PACT depletion had little effect on type I ISG (Hallmark

interferon α response [Liberzon et al. 2015]) expression in HCC1806 or MDA-MB-468 (Supplemental Fig. S3A–C). This observation was verified by qRT-PCR, which again indicated little (<1.7-fold) to no change in ISG expression in PACT depleted cells relative to controls, except for one ISG (*IFIT2*), which was elevated in the PACT-independent cell line MDA-MB-453 upon PACT depletion (Supplemental Fig. S3D). Consistent with the lack of ISG induction in PACT depleted cells, we observed no activation of the OAS-RNase L pathway, which when activated cleaves rRNA leaving behind a distinctive banding pattern that was absent in RNA isolated from PACT depleted HCC1806 and MDA-MB-468 (Supplemental Fig. S3E; Hovanessian and Justesen 2007; Chakrabarti et al. 2011). Taken together, these findings suggest that in PACT-dependent cells, PACT suppresses activation of PKR, but not MDA5, RIG-I, TLR3, or the OASs.

PKR is a well-known activator of the ISR, which is largely facilitated by the transcription factor ATF4 (Gal-Ben-Ari et al. 2018; Costa-Mattioli and Walter 2020). In PACT depleted cells, we observed elevated expression of several ATF4 targets, consistent with activation of ISR, in both our RNA-seq data (Fig. 5C; Supplemental Fig. S4A,B,E; Supplemental Tables S7, S8) and by qRT-PCR (Fig. 5D). Immunoblot analysis confirmed upregulation of the ATF4 targets GADD34 (encoded by *PPP1R15A*) and ATF3 (Fig. 5E,F; Supplemental Fig. S4G). We did not observe robust phosphorylation of eIF2α as would be expected based on the ISR signature in our RNA-seq data and activation of PKR (Fig. 5E,F; Supplemental Fig. S4G). However, GADD34, an eIF2α phosphatase that is expressed during the ISR to dephosphorylate eIF2α to shut down the ISR (Novoa et al. 2001), was highly expressed in our cells at the time of harvest, which could explain the lack of elevated p-eIF2α in PACT depleted cells (Fig. 5E,F).

In addition to the ISR, PKR can also activate the transcription factor NF-κB (Kumar et al. 1994; Gil et al. 1999, 2001; Bonnet et al. 2000, 2006; Zamanian-Daryoush et al. 2000; Chukwurah et al. 2021). Multiple NF-κB targets were upregulated upon PACT depletion in PACT-dependent cell lines as assessed by RNA-seq (Fig. 5C; Supplemental Fig. S4C,D,F; Supplemental Tables S7, S8) and qRT-PCR (Fig. 5G). Immunoblot confirmed phosphorylation of NF-κB p65 (Ser468) in PACT depleted HCC1806 cells (Fig. 5E,F).

Given that PKR activation can drive cell death, we performed a combined depletion experiment to determine if PKR activation is required for cell death upon PACT depletion (Fig. 5H). Depletion of PKR by CRISPR-Cas9 completely rescued the reduced viability caused by depletion of PACT in the PACT-dependent cell line HCC1806 (Fig. 5I). Furthermore, in PKR depleted cells, depletion of PACT did not cause induction of ATF4 or NF-κB target genes (Fig. 5J), indicating that elevated ATF4 and NF-κB target gene expression in PACT depleted cells is entirely dependent on PKR activation.

PACT requires dimerization and dsRNA binding to suppress PKR activation

Multiple proteins suppress activation of PKR through binding to endogenous dsRNAs (Park et al. 1994; Elbarbary et al. 2013; Hu et al. 2023; Cottrell et al. 2024b). For instance, while ADAR1 prevents activation of MDA5 through A-to-I editing, it suppresses PKR activation through competition for dsRNA binding via its dsRBDs (Hu et al. 2023). To determine if dsRNA binding by PACT is required to suppress PKR activation, we performed a rescue experiment in which we overexpressed either wild-type PACT, or two dsRNA binding mutants of PACT. The mutants chosen, PACT-AA and PACT-EAA, were based on previous studies of PACT and ADAR1, in which two or three lysines of the KKxAK motif within their functional dsRBDs (the third dsRBD of PACT does not bind dsRNA [Peters et al. 2001]) had been mutated to abolish dsRNA binding (Fig. 6A; Valente and Nishikura 2007; Takahashi et al. 2013). For both the wild-type and PACT mutants, we made synonymous mutations in the PACT coding sequence to prevent sgRNA binding. Depletion of PACT in empty vector (EV) control HCC1806 (PACT-dependent) cells caused activation of PKR and reduced viability as before (Fig. 6B–D). Both phenotypes were completely rescued by overexpression of wild-type PACT, but neither of the PACT dsRNA binding mutants rescued, indicating that PACT suppresses PKR activation through binding endogenous dsRNAs (Fig. 6B–D). When generating the wild-type and dsRNA binding PACT mutant lines, we observed substantial cell death for the cells transduced with lentivirus for expression of dsRNA binding mutant PACT, but not wild-type PACT (data not shown). Ultimately, the dsRNA binding mutants of PACT were expressed at a much lower level than wild-type overexpression, despite having the same promoter and undergoing the same transduction and selection process in parallel. Despite this difference, the expression of the PACT dsRNA binding mutants is higher than endogenous PACT, and yet is still incapable of rescuing depletion of endogenous PACT.

Like PKR, PACT forms a homodimer, which is facilitated by its third dsRBD (Heyam et al. 2017). To evaluate if dimerization of PACT is required for its ability to suppress PKR activation, we performed another knockout-rescue experiment in HCC1806 with two different PACT constructs. For the first construct, PACT$^{\Delta d3}$, we truncated PACT to remove its third dsRBD, which is required for PACT dimerization (Heyam et al. 2017). To orthogonally restore dimerization of PACT$^{\Delta d3}$, we generated a fusion construct that contained truncated PACT fused to GST to generate PACT$^{\Delta d3}$-GST (Fig. 6E). As GST forms a strong dimer, this construct would be expected to restore dimerization of PACT$^{\Delta d3}$. Like WT PACT, PACT$^{\Delta d3}$ and PACT$^{\Delta d3}$-GST maintained cytoplasmic localization (Supplemental Fig.

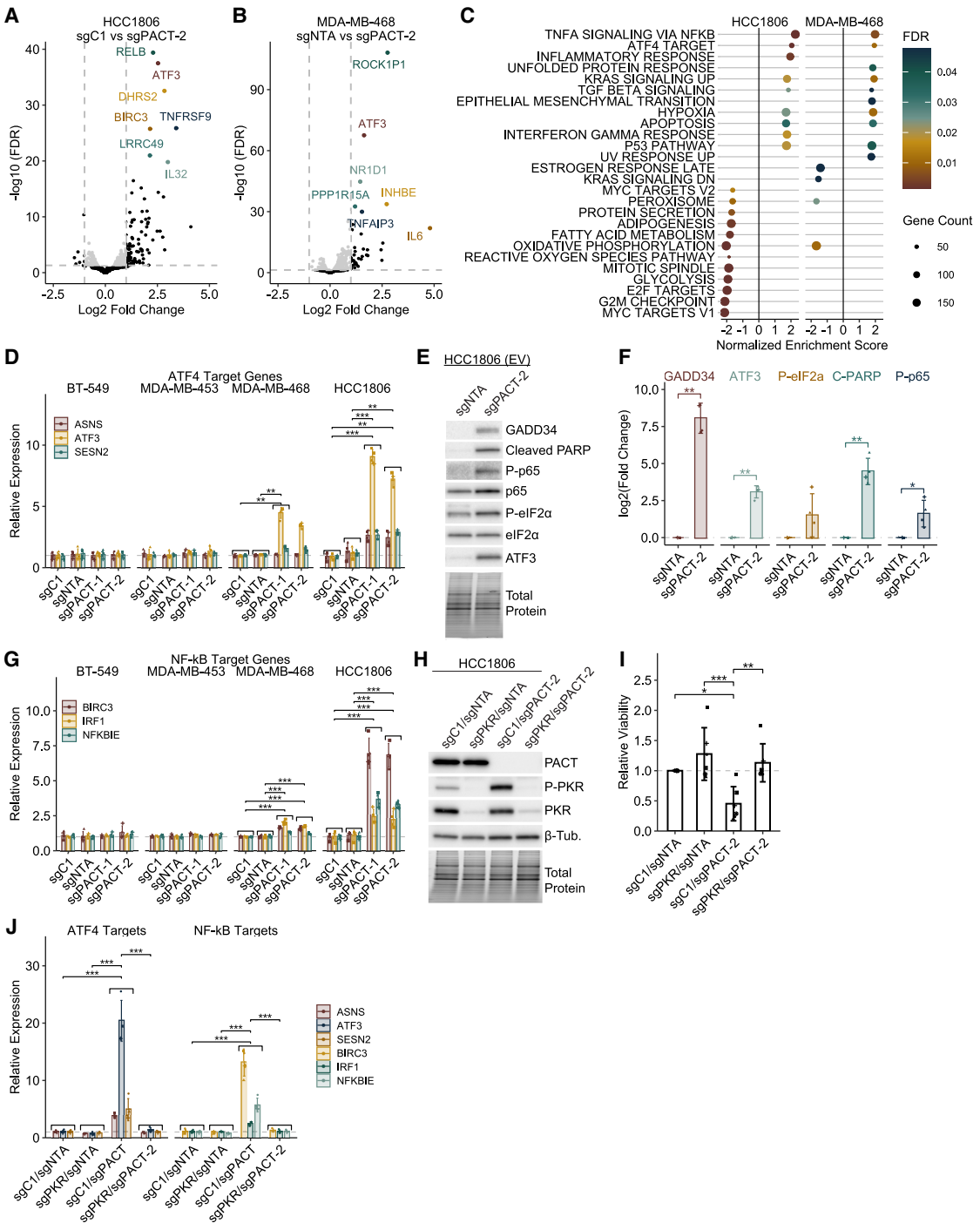

FIGURE 5. PKR is required for activation of NF-κB and ISR upon PACT depletion. (*A*,*B*) Volcano plot for fold change of RNA expression in PACT depleted (sgPACT-2) or control (sgC1 or sgNTA) HCC1806 (*A*) or MDA-MB-468 (*B*). (*C*) Dot plot summarizing the gene sets that are significantly up- or downregulated in PACT depleted cells. FDR is the FDR-corrected *P*-value for each gene set. (*D*,*G*) qRT-PCR for RNA expression for ATF4 targets (*D*) or NF-κB targets (*G*) in PACT depleted and control cells. (*E*) Representative immunoblot of PACT depleted and control HCC1806 EV (empty vector) cells. Total protein was imaged using a stain-free gel and was used as the loading control for normalization. (*F*) Quantification of the immunoblot in *E*. (*H*) Representative immunoblot for HCC1806 control (sgC1/sgNTA), PACT depleted (sgC1/sgPACT-2), PKR depleted (sgC1/sgPKR) or combined depleted cells (sgPKR/sgPACT-2). (*I*) Cell viability as assessed by CellTiter-Glo 2.0 for the same conditions as *H*. (*J*) qRT-PCR for RNA expression for ATF4 targets or NF-κB targets for the same conditions as *H*. Bars represent the average of at least four biological replicates; error bars are ±SD. (*) $P < 0.05$, (**) $P < 0.01$, (***) $P < 0.001$. *P*-values determined by one-way ANOVA with post hoc Tukey for panels *D* and *G* (statistical tests were performed for all genes in the panel as a group, not for individual genes), *t*-test with FDR correction for panel *F*, and by Dunnett's test for panels *I* and *J*.

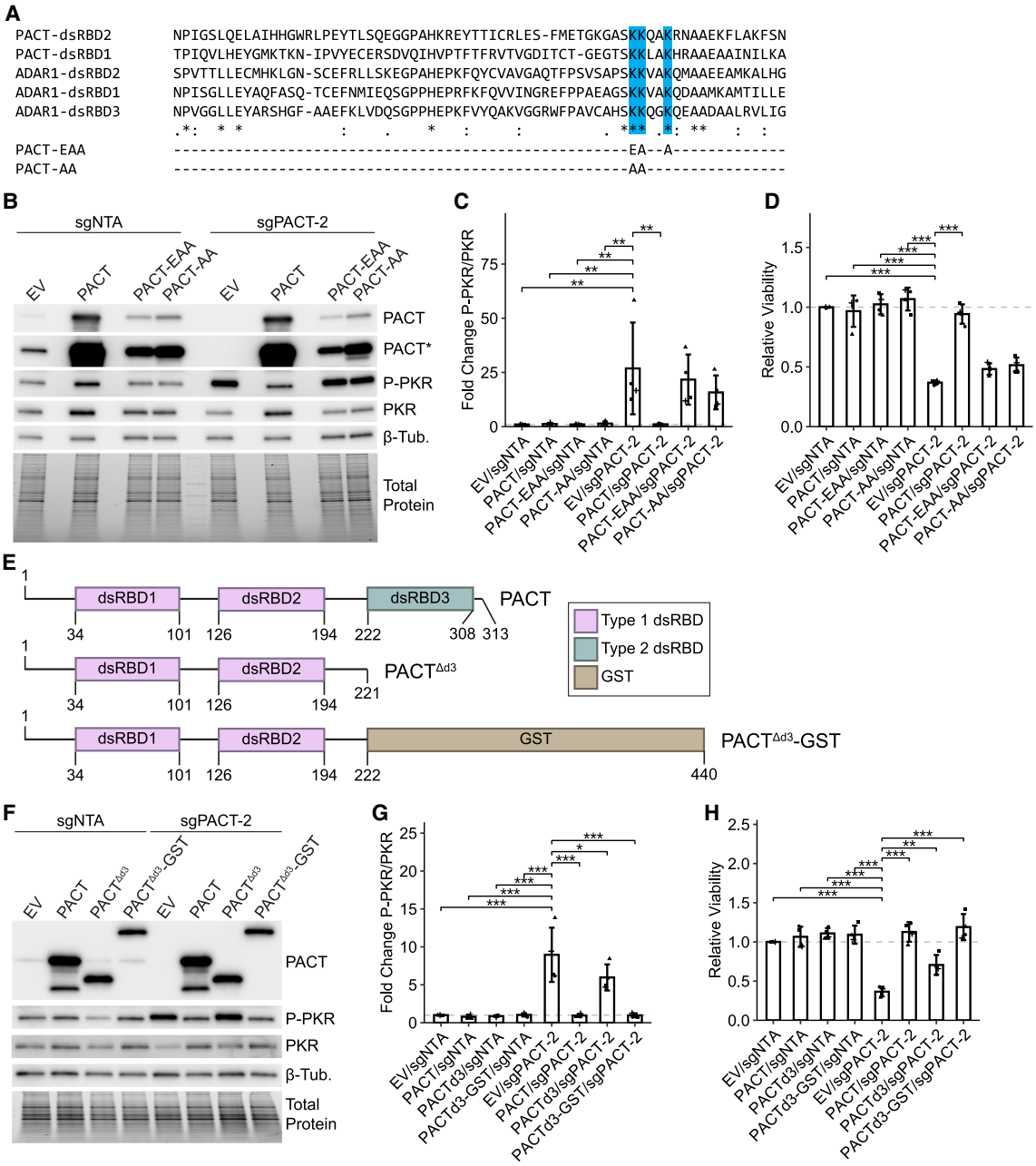

FIGURE 6. PACT dsRNA binding and dimerization is required for suppression of PKR activation. (*A*) Alignment of dsRBD 1 and 2 of PACT and dsRBDs 1–3 of ADAR1. The amino acid substitutions made for disrupting PACT dsRNA binding are shown below. (*B*) Representative immunoblot for HCC1806 control (sgNTA) and PACT depleted (sgPACT-2), with (PACT, PACT-EAA, PACT-AA) or without (EV, empty vector) overexpression of WT or dsRNA binding mutant PACT. The PACT* blot is a longer exposure to show endogenous PACT; see EV-sgNTA lane. (*C*) Quantification of the immunoblots in *B*. (*D*) Cell viability as assessed by CellTiter-Glo 2.0 for the same conditions as *B*. (*E*) Domain structure of WT PACT and PACT truncation and fusion constructs. (*F*) Representative immunoblot for HCC1806 control (sgNTA) and PACT depleted (sgPACT-2), with (PACT, PACT$^{\Delta d3}$, or PACT$^{\Delta d3}$-GST) or without (EV, empty vector) overexpression of WT or truncated PACT. (*G*) Quantification of the immunoblots in *F*. (*H*) Cell viability as assessed by CellTiter-Glo 2.0 for the same conditions as *F*. Bars represent the average of at least three replicates; error bars are ±SD. (*) $P < 0.05$, (**) $P < 0.01$, (***) $P < 0.001$. *P*-values determined by Dunnett's test.

S5A). When expressed in PACT depleted cells, PACT$^{\Delta d3}$ did not rescue PKR activation or fully rescue cell viability (Fig. 6F–H). Conversely, PACT$^{\Delta d3}$-GST, but not GST alone, completely rescued both PKR activation and cell viability (Fig. 6F–H; Supplemental Fig. S5B–D), as well as ISR and NF-κB activation (Supplemental Fig. S5E). These findings indicate that while dsRBD3 is required for suppression of PKR activation, its function regarding suppression of PKR activation is only to allow for dimerization of PACT—which is required to suppress PKR activation.

PACT and ADAR1 redundantly suppress PKR activation in PACT/ADAR1-independent cell lines

Given that *PRKRA* and *ADAR* are codependent genes in many cancer cell lines, and that they both rely on dsRNA binding to suppress PKR activation, we hypothesized that depletion of both ADAR1 and PACT in a PACT/ADAR1-independent cell line would cause activation of PKR. To evaluate that hypothesis, we depleted both PACT and ADAR1, each individually, or neither, in two PACT/ADAR1-independent TNBC cell lines, BT-549 and MDA-MB-453. As in our previous experiments, depletion of PACT alone in both cell lines had little to no effect on cell viability or PKR activation, and we observed the same for depletion of ADAR1 (Fig. 7A–C; Supplemental Fig. S6A,B). Conversely, combined depletion of both ADAR1 and PACT in both cell lines caused robust activation of PKR and for BT-549 reduced viability. Consistent with PKR activation, we observed increased expression of ATF4 targets only in the PACT and ADAR1 depleted cells (Fig. 7D; Supplemental Fig. S6C). Unlike in PACT-dependent cell lines, we did not observe substantial changes in NF-κB target expression (Fig. 7E; Supplemental Fig. S6D). While the expression of most ISGs evaluated remained unchanged upon depletion of PACT and/or ADAR1 in each cell line, the ISG *IFIT2* was upregulated upon PACT depletion in MDA-MB-453 and was further induced in the combined depleted cells (Supplemental Fig. S6E). Finally, we observed no rRNA degradation consistent with OAS/RNase L activation upon depletion of PACT and/or ADAR1 in either cell line (Supplemental Fig. S6F).

To further evaluate redundancy between PACT and ADAR1, we attempted to rescue the effects of PACT depletion in PACT-dependent HCC1806 cells by overexpression of each isoform of ADAR1. Overexpression of either the p110 or p150 isoform of ADAR1 partially rescued PKR activation and reduced viability caused by depletion of PACT in HCC1806 cells (Fig. 7F–H). Taken together with the combined depletion experiments above, these data support a redundant role for PACT and ADAR1 in suppression of PKR activation in PACT/ADAR1-independent cell lines.

PACT-dependency correlates with PKR expression, which is elevated in TNBC

While the data above provide strong evidence to support PACT as a suppressor of PKR activation, they do not explain the differential sensitivity of PACT-dependent and PACT-independent cell lines to depletion of PACT. For ADAR1-dependency, it has been proposed that chronic IFN signaling in ADAR1-dependent cells, which drives elevated expression of the dsRNA sensors MDA5, RIG-I, PKR, and the OASs, sensitizes those cells to depletion of ADAR1 (Liu et al. 2019b). This model likely does not explain PACT-dependency, because unlike ADAR1-dependency, there is no correlation between PACT-dependency score and ISG expression (Fig. 8A,B; Supplemental Fig. S7A,B). By analyzing proteomics data for cancer cell lines, we found that PACT-dependency strongly correlates with PKR expression at the protein level (Fig. 8C; Supplemental Fig. S7C–G). The correlation between PACT-dependency score and PKR protein expression is strongest in breast cancer (Fig. 8D). Consistent with the proteomics and DepMap data, we observed higher PKR expression in PACT-dependent cells relative to PACT-independent cells (Fig. 8E; Supplemental Fig. S7H). Based on mass-spectrometry data, PKR expression is highest in TNBC cell lines (Fig. 8F) and in human tumors, PKR expression at the RNA level is elevated in breast tumors relative to normal breast, with TNBC tumors generally having higher expression (Fig. 8G,H; Supplemental Fig. S7I,J). While not as predictive as PKR expression, it should be noted that the expression of PACT itself correlates with PACT-dependency score (Supplemental Fig. S7K–N).

DISCUSSION

The role of PACT in regulation of PKR has been controversial in the literature. Early reports, which gave PACT its name, provided compelling evidence that PACT functioned to activate PKR through protein–protein interactions in the absence of dsRNA (Patel and Sen 1998; Peters et al. 2001, 2009; Li et al. 2006). Many groups have reported similar findings, often with PACT functioning to activate PKR during stress (Patel et al. 2000; Singh et al. 2011; Farabaugh et al. 2020; Chukwurah et al. 2021). However, other studies indicated that PACT conducts the exact opposite function, inhibiting PKR, including a mouse study showing that PKR (*Eif2ak2*) knockout could rescue embryonic lethality of PACT (Rax in mice, *Prkra*) knockout (Clerzius et al. 2013; Dickerman et al. 2015; Meyer et al. 2018). During the preparation of this manuscript, two studies were published that provided more definitive evidence, consistent with our data here, in support of PACT's role as a suppressor of PKR activation (Ahmad et al. 2025; Manjunath et al. 2025). The cause of the differences between early studies of PACT—those that report on PACT as a PKR activator—versus ours and others' recent findings is not clear. Perhaps the differences could be attributed to technical variables (transfection vs. lentiviral overexpression, overexpression vs. depletion studies), or to unknown biological factors. A possible biological explanation could involve PACT blocking the binding of PKR to endogenous inhibitory RNAs, such as circular RNAs that have been reported to inhibit PKR (Liu et al. 2019a).

While our data indicate that PACT suppresses PKR activation through dimerization and dsRNA binding, the finer details of the mechanism are not clear from our work alone.

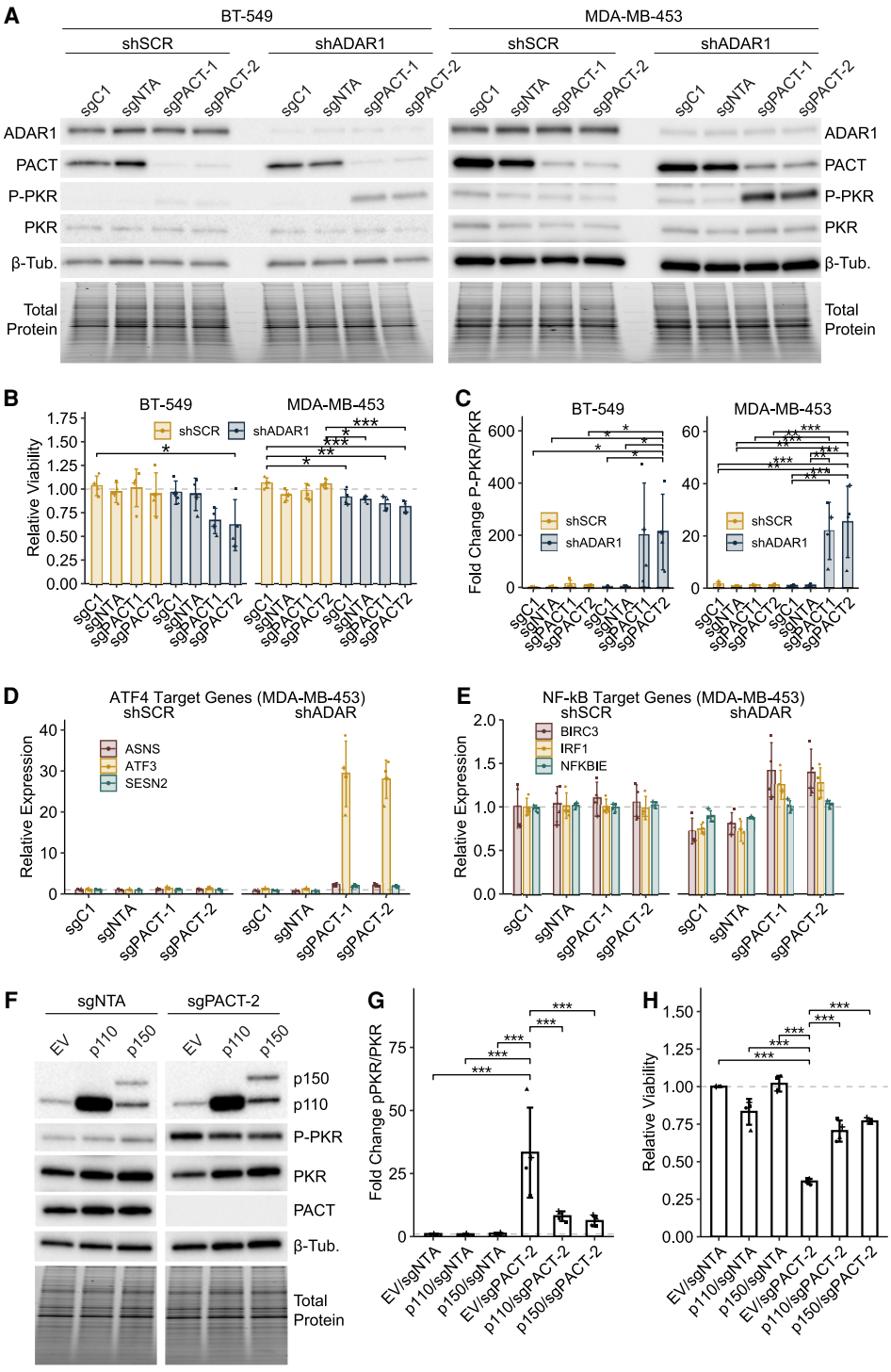

FIGURE 7. PACT and ADAR1 function redundantly to suppress PKR activation in PACT/ADAR1-independent cell lines. (*A*) Representative immunoblot for control (sgC1, sgNTA) and PACT depleted (sgPACT-1, sgPACT-2), with (shADAR1) or without (shSCR) knockdown of ADAR1. (*B*) Cell viability as assessed by CellTiter-Glo 2.0 for the same conditions as *A*. (*C*) Quantification of the immunoblots in *A*. For *B* and *C*, comparisons between sgNTA and sgC1, or sgPACT-1 and sgPACT-2, have been omitted for clarity; plots with those comparisons are in Supplemental Figure S6A, B. (*D*,*E*) qRT-PCR for RNA expression of ATF4 targets (*D*) or NF-κB targets (*E*) for the same conditions as *A*, MDA-MB-453. For panels *D* and *E*, *P*-value annotations have been omitted for clarity; the same data are shown in Supplemental Figure S6C and D with *P*-values annotated. (*F*) Representative immunoblot for control (sgNTA) and PACT depleted (sgPACT-2), with (p110, p150) or without (EV, empty vector) overexpression of ADAR1 isoforms. (*G*) Quantification of the immunoblots in *F*. (*H*) Cell viability as assessed by CellTiter-Glo 2.0 for the same conditions as *F*. Bars represent the average of at least three replicates; error bars are ±SD. (*) $P < 0.05$, (**) $P < 0.01$, (***) $P < 0.001$. *P*-values determined by one-way ANOVA with post hoc Tukey (*B*,*C*) or Dunnett's test (*G*,*H*).

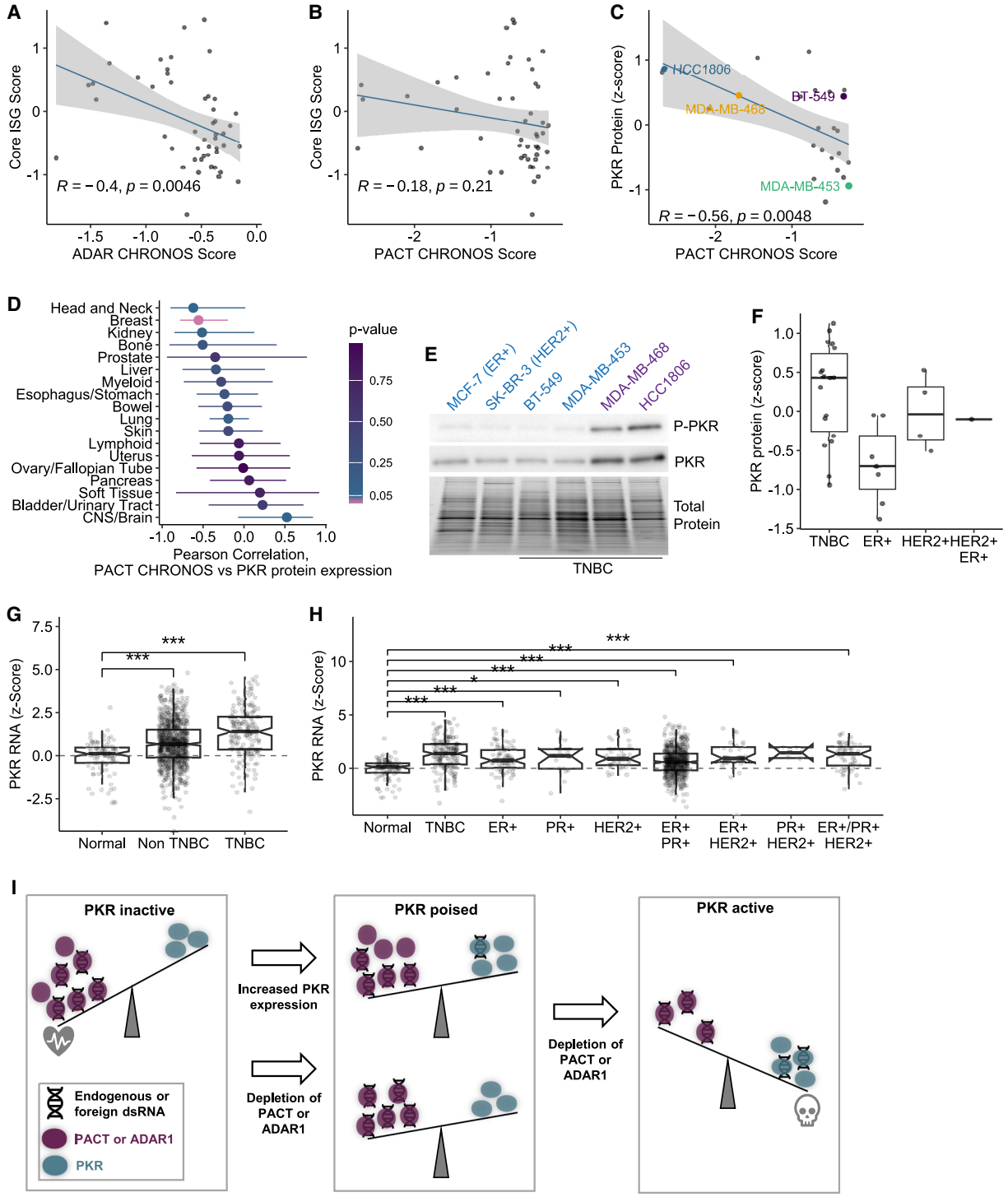

FIGURE 8. PKR expression is elevated in breast cancer and correlates with PACT-dependency. (*A*,*B*) Scatter plots comparing ISG expression (Core ISG score, described previously [Kung et al. 2021]) and either ADAR1-dependency score (ADAR CHRONOS score, *A*) or PACT-dependency score (PACT CHRONOS score, *B*). (*C*) Scatter plot comparing PKR protein abundance and PACT-dependency score. For all scatter plots, the Pearson correlation coefficient and *P*-values are shown. (*D*) Summary of Pearson correlation coefficients and *P*-values between PKR protein abundance and PACT-dependency score for cancer cell line lineages. Lineages with PKR abundance and PACT-dependency scores for fewer than four cell lines were omitted. (*E*) Representative immunoblot for PKR and P-PKR in TNBC cell lines. Total protein is a stain-free gel image used as a loading control. (*F*) PKR protein abundance in breast cancer cell lines separated by subtype. (*G*,*H*) PKR RNA expression in normal human breast and breast tumors; data from TCGA. (*I*) Model for cellular sensitivity to depletion of ADAR1 and/or PACT. For panels *A*–*D* and *F*, data from DepMap; *G* and *H* from TCGA.

Fortunately, another group has examined the mechanism and reported those findings during the preparation of this manuscript (Ahmad et al. 2025). In this work, Ahmad, Zou, Hwang, and Zhao et al. reveal that PACT suppresses PKR activation by preventing dimerization of sliding PKR monomers. Specifically, they propose a model in which weak protein–protein interactions between PKR and PACT prevent sliding of PKR along dsRNA, thus preventing monomers from colliding and forming an active PKR dimer. While that model is supported by our own data showing that PACT requires dsRNA binding to prevent PKR activation, it is not clear how dimerization of PACT fits into the model. A recent study, published during the preparation of this manuscript, found that dimerization of the zebrafish homolog of PACT (Prkra) facilitated binding to and inhibition of eIF2 (Lu et al. 2025). In the model presented with those findings, Prkra uses its third dsRBD to dimerize and sequester eIF2 to inhibit translation, thus assigning a dual role for dsRBD3. Here, we found that dsRBD3 of PACT can be functionally replaced by GST (a dimeric protein), indicating that at least in human cells, dsRBD3's only function in relation to suppression of PKR activity is to facilitate dimerization of PACT. How dimerization enables PKR inhibition is unclear. It is unlikely that dimerization allows PACT to better "compete" with PKR for binding dsRNA as PACT mutants lacking the third dsRBD bind a model dsRNA with the same affinity as full-length PACT (Ahmad et al. 2025). Structural studies are needed to understand the role of dimerization; perhaps dimerization exposes the PKR binding site on PACT, or allows for higher-order structures of PACT-PKR-dsRNA that inhibit or sequester PKR.

Based on the elevated expression of PKR in PACT-dependent cells, we propose a model in which PACT-dependent cells are in a poised state, where because of the elevated abundance of PKR, the cell is highly sensitive to depletion of PACT, and in many cases ADAR1 (Fig. 8I). Conversely, in PACT-independent cell lines, the lower expression of PKR enables either PACT or ADAR1 alone to suppress PKR activation. In these cells, PACT and ADAR1 are functioning redundantly. This shared role of PACT and ADAR1 was also reported in a recent study published during preparation of this manuscript (Manjunath et al. 2025). This redundancy between ADAR1 and PACT is not unique. We have observed the same paradigm before for DHX9 and ADAR1, where depletion of DHX9 in ADAR1-dependent cells causes activation of PKR, while in ADAR1-independent cells, DHX9 and ADAR1 function redundantly to suppress activation of PKR and other dsRNA sensors (Cottrell et al. 2024b). A common thread connecting these proteins is the presence of dsRBDs. Here we show that the dsRNA binding activity of PACT is required for suppression of PKR activation, the same has been observed for ADAR1 previously (Hu et al. 2023), and for DHX9, expression of its dsRBDs alone is sufficient to suppress PKR activation (Cottrell et al. 2024b). While previous cellular studies indicate that ADAR1 suppresses PKR activation by competing with PKR for dsRNA binding, the same was not observed in vitro by Ahmad et al. (Hu et al. 2023; Ahmad et al. 2025). Conversely, Sinigaglia et al. reported a model in which ADAR1-p150 inhibits PKR activation through interaction of its third dsRBD with the kinase domain of PKR while both are bound to dsRNA (Sinigaglia et al. 2024). That model is similar to one proposed by Ahmad et al. in which dsRBD 1 or 2 of PACT interacts with the kinase domain of PKR while both are bound to dsRNA (Ahmad et al. 2025). Further studies are needed to evaluate in finer detail the mechanism by which ADAR1 suppresses PKR activation, and how that may or may not differ from PACT.

More research is also needed to understand the role of ADAR1-p110 in suppressing PKR activation. While both isoforms of ADAR1 can shuttle between the nucleus and cytoplasm, the p150 isoform is generally considered cytoplasmic and the p110 isoform nuclear (Eckmann et al. 2001; Strehblow et al. 2002). Previous literature supports p150 as the ADAR1 isoform that suppresses PKR activation (Chung et al. 2018; Hu et al. 2023), though here we show that overexpression of p110 in PACT depleted cells reduces PKR activation. We have observed something similar in DHX9 and ADAR1 depleted cells, where expression of p110 was capable of suppressing PKR activation (Cottrell et al. 2024b). Additionally, Sinigaglia et al. observed reduced PKR activation upon p110 overexpression in A549 cells (Sinigaglia et al. 2024). It is of course possible that suppression of PKR by p110 in these contexts is an artifact of overexpression and does not occur physiologically. Or perhaps, p110 uses this function in specific contexts when p150 or other proteins are unavailable, possibly in the nucleus (to which some PKR localizes, Supplemental Fig. S5A; Jeffrey et al. 1995) or during mitosis, during which nuclear RNAs can activate PKR (Kim et al. 2014).

Finally, here we provide strong evidence to support the therapeutic targeting of PACT to treat TNBC. There are several attributes that make PACT a good target for TNBC: (1) PACT is highly expressed in TNBC, (2) PACT is essential in many TNBC cell lines, and (3) PKR expression, which correlates with PACT-dependency, is elevated in TNBC. While PACT has no known enzymatic functions, disrupting PACT dimerization would inhibit its regulation of PKR. As such, PACT dimerization inhibitors, or PACT degraders, could have therapeutic potential for TNBC, and likely many other types of cancer.

MATERIALS AND METHODS

Cell culture

Cell lines (MCF-7 [RRID:CVCL_0031], SK-BR-3 [RRID:CVCL_0033], BT-549 [RRID: CVCL_1092], HCC1806 [RRID: CVCL_1258], MDA-MB-468 [RRID: CVCL_0063] MDA-MB-453 [RRID:

CVCL _0418], and 293T [RRID: CVCL_0063]) were obtained from American Type Culture Collection, which used STR profiling to authenticate the cell lines; all cell lines were obtained between 2023 and 2024. The cell lines 293T and SK-BR-3 were cultured in Dulbecco's modified Eagle's medium (DMEM) (HyClone) with 10% fetal bovine serum (Bio-Techne), 2 mM glutamine (HyClone), 0.1 mM nonessential amino acids (HyClone), and 1 mM sodium pyruvate (HyClone). The cell lines MDA-MB-453 and MDA-MB-468 were cultured in Leibovitz L-15 media (HyClone Cat# SH30525) with 10% fetal bovine serum (Bio-Techne). The cell lines HCC1806 and BT-549 were cultured in Roswell Park Memorial Institute 1640 media (Corning Cat# 10-041-CV) with 10% fetal bovine serum (Bio-Techne); for BT-549, recombinant insulin (Gibco) was added to 0.78 µg/mL. The cell line MCF-7 was cultured in modified Eagle's media (HyClone Cat# SH30024.01) with 10% fetal bovine serum (Bio-Techne) and recombinant insulin at 10.2 µg/mL. Except for MDA-MB-453 and MDA-MB-468, all cell lines were grown at 37°C at 5% CO_2, MDA-MB-453 and MDA-MB-468 were grown at 37°C with atmospheric CO_2. Mycoplasma testing was performed by a PCR-based method. All experiments were performed with cells under 20 passages.

Viral production and transduction

Lentivirus was produced by LipoFexin (Lamda Biotech) or polyethylenimine (branched, ~25,000 Da, Sigma-Aldrich) transfection of 293T cells with pCMV-VSV-G (a gift from Bob Weinberg [Stewart et al. 2003], Addgene plasmid #8454; RRID: Addgene_8454) or pMD2.G (a gift from Didier Trono, Addgene plasmid #12259; RRID:Addgene_12259) and pSPAX2 (a gift from Didier Trono, Addgene plasmid #12260; RRID: Addgene_12260), and a transfer plasmid for expression of genes of interest, shRNAs, or sgRNAs. Culture media was changed the day after transfection, and lentivirus containing media was collected the following day, or after 2 days. Lentivirus containing media was filtered through a 0.45 µm filter before transduction of cells of interest in the presence of 10 µg/mL protamine sulfate (Sigma-Aldrich). Depending on the transfer plasmid used and cell line, cells were selected with puromycin at 2 µg/mL (Sigma-Aldrich), 150 µg/mL hygromycin (Gibco or InvivoGen), 10 µg/mL blasticidin (Fisher or InvivoGen), or 500 µg/mL G418 (InvivoGen).

Plasmids

For all sgRNAs targeting genes of interest, oligos encoding the sgRNAs (Supplemental Table S1) were cloned into lentiGuide-puro (a gift from Feng Zhang [Sanjana et al. 2014]), Addgene #52961; RRID:Addgene_52963), lenti-sgRNA-hygro (a gift from Brett Stringer [Stringer et al. 2019], Addgene #104991; RRID: Addgene_ 104991), or tet-pLKO-sgRNA-puro (a gift from Nathanael Gray [Huang et al. 2017], Addgene plasmid # 104321; RRID:Addgene_104321) by ligation of annealed and phosphorylated oligos into a restriction enzyme digested and dephosphorylated vector. The sgRNA sequence for lenti-sgPKR-hygro was used previously (Zou et al. 2024). The pLKO-shSCR-hygro and pLKO-shADAR1-hygro plasmids have been described previously (Cottrell et al. 2024b).

Two control sgRNAs were used in this study. One (sgC1) targets a control genomic locus (AAVS1) and has been used previously (Zou et al. 2024). The second control sgRNA (sgNTA) is a nontargeting sgRNA described previously (Doench et al. 2016). For sgNTA, lentiGuide-sgNTA-puro was purchased from Addgene (a gift from John Doench and David Root [Doench et al. 2016], Addgene plasmid #80248; RRID:Addgene_80248). All other plasmids for the control sgRNAs were cloned in the same manner as described above, and all sequences are available in Supplemental Table S1.

The PACT coding sequence flanked by BamHI and MluI restriction enzyme sites, a Kozak sequence (5′-CACC-3′), and containing wobble mutations to prevent targeting of sgRNAs was synthesized by TwistBio. Restriction enzyme digest and ligation was used to clone PACT into pLV-EF1a-IRES-Blast vector (a gift from Tobias Meyer [Hayer et al. 2016]), Addgene plasmid #85133; RRID: Addgene_85133). The PACT dsRBD mutants were cloned in the same manner; all coding sequences can be found in the Supplemental Information. The PACT-dsRBD3 constructs were made through restriction enzyme digest and ligation. For the $PACT^{\Delta d3}$ plasmid, pLV-EF1a-PACT-IRES-Blast was digested with EcoRI, which cuts between the coding sequence for dsRBD2 and dsRBD3 within PACT, and 3′ of PACT within pLV-EF1a-IRES-Blast. A short double-stranded DNA oligonucleotide encoding two stop codons was ligated in frame with the PACT coding sequence to generate pLV-EF1a-$PACT^{\Delta d3}$-IRES-Blast. The plasmid for $PACT^{\Delta d3}$-GST was cloned in the same manner with GST in place of the oligonucleotide insert. GST was PCR amplified from pDEST15, kindly provided by Dr. Mark Hall, Purdue University, for both the $PACT^{\Delta d3}$-GST and GST alone (pLV-EF1a-GST-Blast) —which was generated by ligation of the GST coding sequence into pLV-EF1a-IRES-Blast, both digested with BamHI and EcoRI. The PCR primers and oligonucleotides used for cloning the PACT-dsRBD3 constructs, as well as the coding sequences of the final constructs, can be found in Supplemental Table S1 and the Supplemental Information. The ADAR1 overexpression constructs used here (pLV-EF1-Blast-p110 and pLV-EF1-Blast-p150) were cloned previously (Cottrell et al. 2024b).

All plasmids were confirmed by restriction enzyme digest, as well as Sanger sequencing and Nanopore whole plasmid sequencing.

Genetic depletion by CRISPR-Cas9

For all CRISPR-Cas9 depletion experiments, the cell lines used in this study were transduced with lentivirus for inducible expression of Cas9 (iCas9) using the transfer plasmid lenti-iCas9-neo (a gift from Qin Yan [Cao et al. 2016], Addgene plasmid # 85400; RRID:Addgene_85400). After transduction and selection with G418, cells with high GFP expression upon doxycycline induction were sorted on a BD FACS Aria by the Purdue Flow Cytometry and Cell Separation Facility. We used either constitutively expressed or inducible sgRNAs targeting genes of interest. For constitutively expressed sgRNAs, we observed premature knockout of the genes of interest in uninduced cells, likely due to "leaky" expression of Cas9. As such, for all experiments using constitutive sgRNA expression (single knockout of PACT in Fig. 4, or combined knockout of PACT and knockdown of ADAR1 in Fig. 8), we began each biological replicate by transducing cells with the lentivirus for sgRNA expression followed by selection and induction with doxycycline. The timelines for transduction, selection,

induction, harvesting of cells, and evaluation of cell viability for each cell line are described in Supplemental Table S2.

For all knockout-rescue experiments and combined knockout of PACT and PKR, we combined iCas9 with an inducible sgRNA construct (tet-pLKO-sgRNA-puro), which prevented knockout prior to induction (data not shown). PACT overexpression and empty vector (EV) control HCC1806-iCas9 cells were generated by lentiviral transduction and selection for transgene incorporation with blasticidin. Subsequently, PACT overexpression and control EV HCC1806-iCas9 lines were transduced with lentivirus made with tet-pLKO-sgPACT-2-puro or tet-pLKO-sgNTA-puro and selected with puromycin. Experimental replicates were initiated by doxycycline treatment, and the timeline is described in Supplemental Table S2. For PKR knockout, HCC1806-iCas9 cells were first transduced with lentivirus made with lenti-sgC1-hygro, lenti-sgPKR-1-hygro or lenti-sgPKR-2-hygro and selected with hygromycin. Cas9 expression was induced by doxycycline, and PKR knockout was confirmed by immunoblot (data not shown). The HCC1806-iCas9 control and PKR knockout lines were passaged without doxycycline before transduction with lentivirus made with tet-pLKO-sgPACT-2-puro or tet-pLKO-sgNTA-puro and selected with puromycin. Experimental replicates were initiated by doxycycline treatment, and the timeline is described in Supplemental Table S2.

Immunoblot

Cell pellets were lysed and sonicated in RIPA buffer (50 mM Tris pH 7.4 [Ambion], 150 mM NaCl [Ambion], 1% Triton X-100 [Sigma-Aldrich], 0.1% sodium dodecyl sulfate [Promega], and 0.5% sodium deoxycholate [Sigma-Aldrich]) with 1× HALT protease and phosphatase inhibitor (Pierce). The DC Assay kit (Bio-Rad) was used to quantify protein concentration. The lysate was diluted in SDS sample buffer (125 mM Tris pH 6.8, 30% glycerol, 10% sodium dodecyl sulfate, 0.012% bromophenol blue) and denatured at 95°C for 7 min. Between 20 and 40 µg of total protein was loaded per lane of 4%–12% TGX Acrylamide Stain-Free gels (Bio-Rad). Prior to transfer by Trans-Blot Turbo (Bio-Rad), the Stain-Free gel was imaged to quantify total protein (Millipore or Bio-Rad). Blots were blocked in 5% milk or 5% bovine serum albumin in Tris-buffered saline with Tween prior to adding primary antibody: ADAR1 (Santa Cruz Biotechnology Cat# sc-73408, RRID:AB_2222767; Bethyl Cat# A303-883A, RRID:AB_2620233), ATF3 (Cell Signaling Technology Cat# 33593, RRID:AB_2799039), eIF2a (Abcam Cat# ab5369, RRID:AB_304838), eIF2a-Ser-51-P (Abcam Cat# ab32157, RRID:AB_732117), GST-Tag (Cell Signaling Technology Cat# 2622, RRID:AB_331670), Phospho-NF-κB p65 (Ser 468) (Cell Signaling Technology Cat# 3039S, RRID:AB_330579), NF-κB p65 (Cell Signaling Technology Cat# 8242S, RRID:AB_10859369), β-tubulin (Abcam Cat# ab6046, RRID:AB_2210370), cleaved PARP (Cell Signaling Technology Cat# 9541, RRID:AB_331426), GADD34 (Cell Signaling Technology Cat# 41222), Histone H3 (Abcam Cat# 10799, RRID:AB_470239), PACT (Cell Signaling Technology Cat# 13490, RRID AB_2798233), PKR (Cell Signaling Technology Cat# 3072, RRID:AB_2277600), PKR Thr-446-P (Abcam Cat# ab32036, RRID:AB_777310). Horseradish-peroxidase conjugated secondary antibodies (Jackson ImmunoResearch) and Clarity Western ECL Substrate (Bio-Rad) were used for detection via ChemiDoc (Bio-Rad). Image Lab (Bio-Rad) was used to determine band intensities, which were normalized to total protein measured by imaging of the Stain-Free gel.

Cell viability and crystal violet staining

For cell viability assessment, 5000 cells were plated in triplicate for each condition in opaque white 96-well plates. Cell viability was assessed by CellTiter-Glo 2.0 (Promega) per manufacturer's protocol between 3 and 4 days after plating. For details on the number of cells plated and the timeline for cell viability assessment, see Supplemental Table S2.

For crystal violet staining, 2000 cells were plated per well of a 6-well dish. Between 15 and 20 days later, cells were washed briefly with 1× PBS prior to fixation in 100% methanol for 5 min. After drying, the cells were stained with 0.005% Crystal Violet solution containing 25% methanol (Sigma-Aldrich) prior to washing excess stain away with deionized water. Plates were imaged using a Bio-Rad ChemiDoc.

Tumorigenesis

The Biological Evaluation Shared Resource at Purdue University Institute for Cancer Research performed the tumorigenesis study. From the cranial end, the second left ventral mammary fat-pad of female NRG (NOD.Cg-Rag1tm1Mom Il2rgtm1Wjl/SzJ) mice, originally obtained from The Jackson Laboratory (RRID:IMSR_JAX:007799), were injected with 2.9×10^6 HCC1806 cells suspended in equal volumes of 1× PBS and Matrigel (Corning). Five days after injection, when tumors were palpable, mice were given their normal acidified drinking water supplemented with 2.4 mg/mL doxycycline. Tumor volume was measured manually using a caliper 3 days per week until the first mouse reached a humane euthanasia criterion. Five mice were injected per condition; one mouse injected with the sgNTA line was euthanized early due to poor health.

RNA purification and analysis of rRNA integrity

RNA was purified using the Nucleospin RNA kit (MACHEREY-NAGEL). Ribosomal RNA integrity was determined using an Agilent TapeStation by the Genomics and Genome Editing Facility at Purdue University.

RNA sequencing and analysis

Contaminating DNA was removed from total RNA by TURBO DNase (Thermo Fisher Scientific) prior to rRNA depletion using QIAseq FastSelect–rRNA HMR kit (QIAGEN) per the manufacturer's protocol. RNA sequencing libraries were constructed with the NEBNext Ultra II RNA Library Preparation Kit for Illumina per the manufacturer's recommendations. Sequencing libraries were validated by Agilent TapeStation 4200 and quantified by Qubit 2.0 Fluorometer (Thermo Fisher Scientific) as well as by quantitative PCR (Kapa Biosystems). The sequencing libraries were multiplexed and clustered onto a flowcell on the Illumina NovaSeq instrument. The samples were sequenced using a 2 × 150 bp

paired-end configuration. Image analysis and base calling were conducted by NovaSeq Control Software. Raw sequence data (.bcl files) generated from Illumina NovaSeq were converted into FASTQ files and demultiplexed using Illumina bcl2fastq 2.20 software. One mismatch was allowed for index sequence identification.

Sequence reads were processed using Trimmomatic v.0.36 to remove adapter sequences and poor-quality nucleotides. Trimmed reads were aligned to GRCh38 reference genome using STAR aligner v2.5.2b (RRID:SCR_004463). Gene counts were determined using featureCounts from Subread v.1.5.2 (RRID:SCR_009803); only unique exonic reads were counted. Differential gene expression was determined using DESeq2 (RRID:SCR_015687, see Data Availability below for scripts) with shrunken fold changes using the "apeglm" method (Zhu et al. 2019). Gene set enrichment analysis was performed using "clusterProfiler" (RRID:SCR_016884) with Gene Ontology (RRID:SCR_002811) terms from Ashburner et al. (2000) and Aleksander et al. (2023) or Hallmark gene sets from the Molecular Signatures Database (RRID:SCR_016863) (Liberzon et al. 2015). For Gene Set Enrichment Analysis with Hallmark gene sets, an additional gene set was included for previously identified ATF4 target genes (Wong et al. 2019).

Quantitative PCR

LunaScript Supermix (NEB) was used to make cDNA for quantitative PCR (qPCR), using Luna Universal qPCR MasterMix (NEB) on a QuantStudio3 system (Thermo Scientific). All primers used for qPCR are listed in Supplemental Table S1. The amplification efficiency of each primer was verified to be within 90%–110% allowing determination of "Fold Change" by the $\Delta\Delta C_t$. Two reference genes were used for normalization, EEF1A1 and HSPA5, using their geometric mean *Ct* for calculating ΔC_t.

Analysis of TCGA data

For TCGA data, normalization of RNA-seq data, and *Z*-scores calculations were performed as previously described (Kung et al. 2021). Breast cancer cell lines and TCGA tumor molecular subtypes were defined previously (Lehmann et al. 2016). The R packages RTCGA and survminer (RRID:SCR_021094) were used to determine breast cancer survival. The surv_cutpoint function of survminer was used to determine an expression cutoff.

DATA DEPOSITION

All analysis scripts are available at https://github.com/cottrellka/Young_et_al_2025. Raw RNA-seq and gene count data is available at the Gene Expression Omnibus (GSE298233). Dependency (DepMap_Public_24Q4+Score,_Chronos, and Achilles +DRIVE+Marcotte,_DEMETER2), transcriptomic (Batch_corrected_Expression_Public_24Q4) and proteomic data for cancer cell lines (Harmonized_MS_CCLE_Gygi) were obtained from the DepMap portal (https://depmap.org/portal/download/custom/, RRID:SCR_017655). Transcriptomic data for TCGA BRCA samples (illuminahiseq_rnaseqv2-RSEM_genes) and clinical data (Merge_Clinical) were obtained from the Broad Institute FireBrowse and are available at http://firebrowse.org/.

SUPPLEMENTAL MATERIAL

Supplemental material is available for this article.

ACKNOWLEDGMENTS

The data described here are in part based on data generated by the TCGA Research Network: https://www.cancer.gov/tcga. This work was supported by R00MD016946 (K.A. Cottrell), the Ralph W. and Grace M. Showalter Research Trust award (K.A. Cottrell), the Purdue Institute for Cancer Research (startup funding, Robbers New Investigator Award to K.A. Cottrell, and support for the Biological Evaluation Shared Resource) NIH grant P30CA023168, and startup funding from Purdue University Department of Biochemistry and College of Agriculture. Jill Hutchcroft, director of the Flow Cytometry and Cell Separation Facility at Purdue University, for sorting iCas9 cell lines. Cottrell Lab rotation students Jolene Mach, Geethma Lirushie, Nima Goodarzi, Ayomide Adebesin, Yalan Huo, Troy Sievertsen, Tommy Sheeley, and Reed Smith.

Author contributions: K.A.C. and A.A.Y. conceived the project. K.A.C., A.A.Y., and B.D.E. designed the experiments. A.A.Y., K.A.C., I.G.J., J.R.P., H.E.B., H.A.H., D.S.O., R.N.C., M.E.L., and E.N.G. performed the experiments and/or provided materials. K.A.C., A.A.Y., I.G.J., J.R.P., and H.E.B. performed the data analysis. K.A.C., A.A.Y., and I.G.J. wrote the manuscript. All authors edited the manuscript.

Received June 10, 2025; accepted July 26, 2025.

REFERENCES

Ahmad S, Zou T, Hwang J, Zhao L, Wang X, Davydenko A, Buchumenski I, Zhuang P, Fishbein AR, Capcha-Rodriguez D, et al. 2025. PACT prevents aberrant activation of PKR by endogenous dsRNA without sequestration. *Nat Commun* **16:** 3325. doi:10.1038/s41467-025-58433-x

Aleksander SA, Balhoff J, Carbon S, Cherry JM, Drabkin HJ, Ebert D, Feuermann M, Gaudet P, Harris NL, Hill DP, et al. 2023. The Gene Ontology knowledgebase in 2023. *Genetics* **224:** iyad031. doi:10.1093/genetics/iyad031

Arafeh R, Shibue T, Dempster JM, Hahn WC, Vazquez F. 2025. The present and future of the Cancer Dependency Map. *Nature Rev Cancer* **25:** 59–73. doi:10.1038/s41568-024-00763-x

Ashburner M, Ball CA, Blake JA, Botstein D, Butler H, Cherry JM, Davis AP, Dolinski K, Dwight SS, Eppig JT, et al. 2000. Gene ontology: tool for the unification of biology. The Gene Ontology Consortium. *Nat Genet* **25:** 25–29. doi:10.1038/75556

Bass BL. 2024. Adenosine deaminases that act on RNA, then and now. *RNA* **30:** 521–529. doi:10.1261/rna.079990.124

Bass BL, Weintraub H. 1988. An unwinding activity that covalently modifies its double-stranded RNA substrate. *Cell* **55:** 1089–1098. doi:10.1016/0092-8674(88)90253-X

Bianchini G, Balko JM, Mayer IA, Sanders ME, Gianni L. 2016. Triple-negative breast cancer: challenges and opportunities of a heterogeneous disease. *Nat Rev Clin Oncol* **13:** 674–690. doi:10.1038/nrclinonc.2016.66

Bonnet MC, Weil R, Dam E, Hovanessian AG, Meurs EF. 2000. PKR stimulates NF-κB irrespective of its kinase function by interacting with the IκB kinase complex. *Mol Cell Biol* **20:** 4532–4542. doi:10.1128/MCB.20.13.4532-4542.2000

Bonnet MC, Daurat C, Ottone C, Meurs EF. 2006. The N-terminus of PKR is responsible for the activation of the NF-κB signaling pathway by interacting with the IKK complex. *Cell Signal* **18:** 1865–1875. doi:10.1016/j.cellsig.2006.02.010

Cao J, Wu L, Zhang SM, Lu M, Cheung WK, Cai W, Gale M, Xu Q, Yan Q. 2016. An easy and efficient inducible CRISPR/Cas9 platform with improved specificity for multiple gene targeting. *Nucleic Acids Res* **44:** e149. doi:10.1093/nar/gkw660

Chakrabarti A, Jha BK, Silverman RH. 2011. New insights into the role of RNase L in innate immunity. *J Interferon Cytokine Res* **31:** 49–57. doi:10.1089/jir.2010.0120

Chen YG, Hur S. 2022. Cellular origins of dsRNA, their recognition and consequences. *Nat Rev Mol Cell Biol* **23:** 286–301. doi:10.1038/s41580-021-00430-1

Chen DS, Mellman I. 2017. Elements of cancer immunity and the cancer-immune set point. *Nature* **541:** 321–330. doi:10.1038/nature21349

Chen R, Ishak CA, De Carvalho DD. 2021. Endogenous retroelements and the viral mimicry response in cancer therapy and cellular homeostasis. *Cancer Discov* **11:** 2707–2725. doi:10.1158/2159-8290.CD-21-0506

Chukwurah E, Farabaugh KT, Guan BJ, Ramakrishnan P, Hatzoglou M. 2021. A tale of two proteins: PACT and PKR and their roles in inflammation. *FEBS J* **288:** 6365–6391. doi:10.1111/febs.15691

Chung H, Calis JJA, Wu X, Sun T, Yu Y, Sarbanes SL, Dao Thi VL, Shilvock AR, Hoffmann HH, Rosenberg BR, et al. 2018. Human ADAR1 prevents endogenous RNA from triggering translational shutdown. *Cell* **172:** 811–824.e4. doi:10.1016/j.cell.2017.12.038

Clerzius G, Shaw E, Daher A, Burugu S, Gélinas JF, Ear T, Sinck L, Routy JP, Mouland AJ, Patel RC, et al. 2013. The PKR activator, PACT, becomes a PKR inhibitor during HIV-1 replication. *Retrovirology* **10:** 96. doi:10.1186/1742-4690-10-96

Costa-Mattioli M, Walter P. 2020. The integrated stress response: from mechanism to disease. *Science* **368:** eaat5314. doi:10.1126/science.aat5314

Cottrell KA, Andrews RJ, Bass BL. 2024a. The competitive landscape of the dsRNA world. *Mol Cell* **84:** 107–119. doi:10.1016/j.molcel.2023.11.033

Cottrell KA, Ryu S, Pierce JR, Soto Torres L, Bohlin HE, Schab AM, Weber JD. 2024b. Induction of viral mimicry upon loss of DHX9 and ADAR1 in breast cancer cells. *Cancer Res Commun* **4:** 986–1003. doi:10.1158/2767-9764.CRC-23-0488

Curigliano G, Goldhirsch A. 2011. The triple-negative subtype: new ideas for the poorest prognosis breast cancer. *J Natl Cancer Inst Monogr* **2011:** 108–110. doi:10.1093/jncimonographs/lgr038

Dempster JM, Rossen J, Kazachkova M, Pan J, Kugener G, Root DE, Tsherniak A. 2019. Extracting biological insights from the Project Achilles genome-scale CRISPR screens in cancer cell lines. bioRxiv. doi:10.1101/720243

Dickerman BK, White CL, Kessler PM, Sadler AJ, Williams BR, Sen GC. 2015. The protein activator of protein kinase R, PACT/RAX, negatively regulates protein kinase R during mouse anterior pituitary development. *FEBS J* **282:** 4766–4781. doi:10.1111/febs.13533

Doench JG, Fusi N, Sullender M, Hegde M, Vaimberg EW, Donovan KF, Smith I, Tothova Z, Wilen C, Orchard R, et al. 2016. Optimized sgRNA design to maximize activity and minimize off-target effects of CRISPR-Cas9. *Nat Biotechnol* **34:** 184–191. doi:10.1038/nbt.3437

Eckmann CR, Neunteufl A, Pfaffstetter L, Jantsch MF. 2001. The human but not the *Xenopus* RNA-editing enzyme ADAR1 has an atypical nuclear localization signal and displays the characteristics of a shuttling protein. *Mol Biol Cell* **12:** 1911–1924. doi:10.1091/mbc.12.7.1911

Elbarbary RA, Li W, Tian B, Maquat LE. 2013. STAU1 binding 3′ UTR IRA*lus* complements nuclear retention to protect cells from PKR-mediated translational shutdown. *Genes Dev* **27:** 1495–1510. doi:10.1101/gad.220962.113

Farabaugh KT, Krokowski D, Guan BJ, Gao Z, Gao XH, Wu J, Jobava R, Ray G, de Jesus TJ, Bianchi MG, et al. 2020. PACT-mediated PKR activation acts as a hyperosmotic stress intensity sensor weakening osmoadaptation and enhancing inflammation. *eLife* **9:** e52241. doi:10.7554/eLife.52241

Gal-Ben-Ari S, Barrera I, Ehrlich M, Rosenblum K. 2018. PKR: a kinase to remember. *Front Mol Neurosci* **11:** 480. doi:10.3389/fnmol.2018.00480

Gannon HS, Zou T, Kiessling MK, Gao GF, Cai D, Choi PS, Ivan AP, Buchumenski I, Berger AC, Goldstein JT, et al. 2018. Identification of ADAR1 adenosine deaminase dependency in a subset of cancer cells. *Nat Commun* **9:** 5450. doi:10.1038/s41467-018-07824-4

Gil J, Alcamí J, Esteban M. 1999. Induction of apoptosis by double-stranded-RNA-dependent protein kinase (PKR) involves the alpha subunit of eukaryotic translation initiation factor 2 and NF-κB. *Mol Cell Biol* **19:** 4653–4663. doi:10.1128/MCB.19.7.4653

Gil J, Rullas J, García MA, Alcamí J, Esteban M. 2001. The catalytic activity of dsRNA-dependent protein kinase, PKR, is required for NF-κB activation. *Oncogene* **20:** 385–394. doi:10.1038/sj.onc.1204109

Guirguis AA, Ofir-Rosenfeld Y, Knezevic K, Blackaby W, Hardick D, Chan YC, Motazedian A, Gillespie A, Vassiliadis D, Lam EYN, et al. 2023. Inhibition of METTL3 results in a cell-intrinsic interferon response that enhances antitumor immunity. *Cancer Discov* **13:** 2228–2247. doi:10.1158/2159-8290.CD-23-0007

Hayer A, Shao L, Chung M, Joubert L-M, Yang HW, Tsai F-C, Bisaria A, Betzig E, Meyer T. 2016. Engulfed cadherin fingers are polarized junctional structures between collectively migrating endothelial cells. *Nat Cell Biol* **18:** 1311–1323. doi:/10.1038/ncb3438

Heyam A, Coupland CE, Dégut C, Haley RA, Baxter NJ, Jakob L, Aguiar PM, Meister G, Williamson MP, Lagos D, et al. 2017. Conserved asymmetry underpins homodimerization of Dicer-associated double-stranded RNA-binding proteins. *Nucleic Acids Res* **45:** 12577–12584. doi:10.1093/nar/gkx928

Hovanessian AG, Justesen J. 2007. The human 2′-5′ oligoadenylate synthetase family: unique interferon-inducible enzymes catalyzing 2′-5′ instead of 3′-5′ phosphodiester bond formation. *Biochimie* **89:** 779–788. doi:10.1016/j.biochi.2007.02.003

Hu SB, Heraud-Farlow J, Sun T, Liang Z, Goradia A, Taylor S, Walkley CR, Li JB. 2023. ADAR1p150 prevents MDA5 and PKR activation via distinct mechanisms to avert fatal autoinflammation. *Mol Cell* **83:** 3869–3884.e7. doi:10.1016/j.molcel.2023.09.018

Huang HT, Seo HS, Zhang T, Wang Y, Jiang B, Li Q, Buckley DL, Nabet B, Roberts JM, Paulk J, et al. 2017. MELK is not necessary for the proliferation of basal-like breast cancer cells. *eLife* **6:** e26693. doi:10.7554/eLife.26693

Huang W, Zhu Q, Shi Z, Tu Y, Li Q, Zheng W, Yuan Z, Li L, Zu X, Hao Y, et al. 2024. Dual inhibitors of DNMT and HDAC induce viral mimicry to induce antitumour immunity in breast cancer. *Cell Death Discov* **10:** 143. doi:10.1038/s41420-024-01895-7

Ishizuka JJ, Manguso RT, Cheruiyot CK, Bi K, Panda A, Iracheta-Vellve A, Miller BC, Du PP, Yates KB, Dubrot J, et al. 2019. Loss of ADAR1 in tumours overcomes resistance to immune checkpoint blockade. *Nature* **565:** 43–48. doi:10.1038/s41586-018-0768-9

Jeffrey IW, Kadereit S, Meurs EF, Metzger T, Bachmann M, Schwemmle M, Hovanessian AG, Clemens MJ. 1995. Nuclear

localization of the interferon-inducible protein kinase PKR in human cells and transfected mouse cells. *Exp Cell Res* **218:** 17–27. doi:10.1006/excr.1995.1126

Jiang X, Muthusamy V, Fedorova O, Kong Y, Kim DJ, Bosenberg M, Pyle AM, Iwasaki A. 2019. Intratumoral delivery of RIG-I agonist SLR14 induces robust antitumor responses. *J Exp Med* **216:** 2854–2868. doi:10.1084/jem.20190801

Kim Y, Lee JH, Park JE, Cho J, Yi H, Kim VN. 2014. PKR is activated by cellular dsRNAs during mitosis and acts as a mitotic regulator. *Genes Dev* **28:** 1310–1322. doi:10.1101/gad.242644.114

Kumar A, Haque J, Lacoste J, Hiscott J, Williams BR. 1994. Double-stranded RNA-dependent protein kinase activates transcription factor NF-κB by phosphorylating IκB. *Proc Natl Acad Sci* **91:** 6288–6292. doi:10.1073/pnas.91.14.6288

Kung CP, Cottrell KA, Ryu S, Bramel ER, Kladney RD, Bao EA, Freeman EC, Sabloak T, Maggi L, Weber JD. 2021. Evaluating the therapeutic potential of ADAR1 inhibition for triple-negative breast cancer. *Oncogene* **40:** 189–202. doi:10.1038/s41388-020-01515-5

Lehmann BD, Jovanović B, Chen X, Estrada MV, Johnson KN, Shyr Y, Moses HL, Sanders ME, Pietenpol JA. 2016. Refinement of triple-negative breast cancer molecular subtypes: implications for neoadjuvant chemotherapy selection. *PLoS One* **11:** e0157368. doi:10.1371/journal.pone.0157368

Li S, Peters GA, Ding K, Zhang X, Qin J, Sen GC. 2006. Molecular basis for PKR activation by PACT or dsRNA. *Proc Natl Acad Sci* **103:** 10005–10010. doi:10.1073/pnas.0602317103

Liberzon A, Birger C, Thorvaldsdóttir H, Ghandi M, Mesirov JP, Tamayo P. 2015. The Molecular Signatures Database (MSigDB) hallmark gene set collection. *Cell Syst* **1:** 417–425. doi:10.1016/j.cels.2015.12.004

Liddicoat BJ, Piskol R, Chalk AM, Ramaswami G, Higuchi M, Hartner JC, Li JB, Seeburg PH, Walkley CR. 2015. RNA editing by ADAR1 prevents MDA5 sensing of endogenous dsRNA as non-self. *Science* **349:** 1115–1120. doi:10.1126/science.aac7049

Liu CX, Li X, Nan F, Jiang S, Gao X, Guo SK, Xue W, Cui Y, Dong K, Ding H, et al. 2019a. Structure and degradation of circular RNAs regulate PKR activation in innate immunity. *Cell* **177:** 865–880.e21. doi:10.1016/j.cell.2019.03.046

Liu H, Golji J, Brodeur LK, Chung FS, Chen JT, deBeaumont RS, Bullock CP, Jones MD, Kerr G, Li L, et al. 2019b. Tumor-derived IFN triggers chronic pathway agonism and sensitivity to ADAR loss. *Nat Med* **25:** 95–102. doi:10.1038/s41591-018-0302-5

Lu T, Ma P, Fang H, Chen A, Xu J, Kuang X, Wang M, Su L, Wang S, Zhang Y, et al. 2025. Prkra dimer senses double-stranded RNAs to dictate global translation efficiency. *Mol Cell* **85:** 2032–2047.e9. doi:10.1016/j.molcel.2025.04.005

Manjunath L, Santiago G, Ortega P, Sanchez A, Oh S, Garcia A, Li J, Duong D, Bournique E, Bouin A, et al. 2025. Cooperative role of PACT and ADAR1 in preventing aberrant PKR activation by self-derived double-stranded RNA. *Nat Commun* **16:** 3246. doi:10.1038/s41467-025-58412-2

Mannion NM, Greenwood SM, Young R, Cox S, Brindle J, Read D, Nellåker C, Vesely C, Ponting Chris P, McLaughlin Paul J, et al. 2014. The RNA-editing enzyme ADAR1 controls innate immune responses to RNA. *Cell Rep* **9:** 1482–1494. doi:10.1016/j.celrep.2014.10.041

Matsumoto M, Oshiumi H, Seya T. 2011. Antiviral responses induced by the TLR3 pathway. *Rev Med Virol* **21:** 67–77. doi:10.1002/rmv.680

McFarland JM, Ho ZV, Kugener G, Dempster JM, Montgomery PG, Bryan JG, Krill-Burger JM, Green TM, Vazquez F, Boehm JS, et al. 2018. Improved estimation of cancer dependencies from large-scale RNAi screens using model-based normalization and data integration. *Nat Commun* **9:** 4610. doi:10.1038/s41467-018-06916-5

Mendoza HG, Beal PA. 2024. Structural and functional effects of inosine modification in mRNA. *RNA* **30:** 512–520. doi:10.1261/rna.079977.124

Meyer C, Garzia A, Mazzola M, Gerstberger S, Molina H, Tuschl T. 2018. The TIA1 RNA-binding protein family regulates EIF2AK2-mediated stress response and cell cycle progression. *Mol Cell* **69:** 622–635.e6. doi:10.1016/j.molcel.2018.01.011

Morad G, Helmink BA, Sharma P, Wargo JA. 2021. Hallmarks of response, resistance, and toxicity to immune checkpoint blockade. *Cell* **184:** 5309–5337. doi:10.1016/j.cell.2021.09.020

Novoa I, Zeng H, Harding HP, Ron D. 2001. Feedback inhibition of the unfolded protein response by *GADD34*-mediated dephosphorylation of eIF2α. *J Cell Biol* **153:** 1011–1022. doi:10.1083/jcb.153.5.1011

Park H, Davies MV, Langland JO, Chang HW, Nam YS, Tartaglia J, Paoletti E, Jacobs BL, Kaufman RJ, Venkatesan S. 1994. TAR RNA-binding protein is an inhibitor of the interferon-induced protein kinase PKR. *Proc Natl Acad Sci* **91:** 4713–4717. doi:10.1073/pnas.91.11.4713

Patel RC, Sen GC. 1998. PACT, a protein activator of the interferon-induced protein kinase, PKR. *EMBO J* **17:** 4379–4390. doi:10.1093/emboj/17.15.4379

Patel CV, Handy I, Goldsmith T, Patel RC. 2000. PACT, a stress-modulated cellular activator of interferon-induced double-stranded RNA-activated protein kinase, PKR. *J Biol Chem* **275:** 37993–37998. doi:10.1074/jbc.M004762200

Pestal K, Funk CC, Snyder JM, Price ND, Treuting PM, Stetson DB. 2015. Isoforms of RNA-editing enzyme ADAR1 independently control nucleic acid sensor MDA5-driven autoimmunity and multi-organ development. *Immunity* **43:** 933–944. doi:10.1016/j.immuni.2015.11.001

Peters GA, Hartmann R, Qin J, Sen GC. 2001. Modular structure of PACT: distinct domains for binding and activating PKR. *Mol Cell Biol* **21:** 1908–1920. doi:10.1128/MCB.21.6.1908-1920.2001

Peters GA, Dickerman B, Sen GC. 2009. Biochemical analysis of PKR activation by PACT. *Biochemistry* **48:** 7441–7447. doi:10.1021/bi900433y

Rehwinkel J, Gack MU. 2020. RIG-I-like receptors: their regulation and roles in RNA sensing. *Nat Rev Immunol* **20:** 537–551. doi:10.1038/s41577-020-0288-3

Sanjana NE, Shalem O, Zhang F. 2014. Improved vectors and genome-wide libraries for CRISPR screening. *Nat Methods* **11:** 783–784. doi:/10.1038/nmeth.3047

Singh M, Castillo D, Patel CV, Patel RC. 2011. Stress-induced phosphorylation of PACT reduces its interaction with TRBP and leads to PKR activation. *Biochemistry* **50:** 4550–4560. doi:10.1021/bi200104h

Sinigaglia K, Cherian A, Du Q, Lacovich V, Vukić D, Melicherová J, Linhartova P, Zerad L, Stejskal S, Malik R, et al. 2024. An ADAR1 dsRBD3-PKR kinase domain interaction on dsRNA inhibits PKR activation. *Cell Rep* **43:** 114618. doi:10.1016/j.celrep.2024.114618

Stewart SA, Dykxhoorn DM, Palliser D, Mizuno H, Yu EY, An DS, Sabatini DM, Chen IS, Hahn WC, Sharp PA, et al. 2003. Lentivirus-delivered stable gene silencing by RNAi in primary cells. *RNA* **9:** 493–501. doi:10.1261/rna.2192803

Strehblow A, Hallegger M, Jantsch MF. 2002. Nucleocytoplasmic distribution of human RNA-editing enzyme ADAR1 is modulated by double-stranded RNA-binding domains, a leucine-rich export signal, and a putative dimerization domain. *Mol Biol Cell* **13:** 3822–3835. doi:10.1091/mbc.e02-03-0161

Stringer BW, Day BW, D'Souza RCJ, Jamieson PR, Ensbey KS, Bruce ZC, Lim YC, Goasdoué K, Offenhäuser C, Akgül S, et al. 2019. A reference collection of patient-derived cell line and

xenograft models of proneural, classical and mesenchymal glioblastoma. *Sci Rep* **9:** 4902. doi:10.1038/s41598-019-41277-z

Takahashi T, Miyakawa T, Zenno S, Nishi K, Tanokura M, Ui-Tei K. 2013. Distinguishable in vitro binding mode of monomeric TRBP and dimeric PACT with siRNA. *PLoS One* **8:** e63434. doi:10.1371/journal.pone.0063434

Valente L, Nishikura K. 2007. RNA binding-independent dimerization of adenosine deaminases acting on RNA and dominant negative effects of nonfunctional subunits on dimer functions. *J Biol Chem* **282:** 16054–16061. doi:10.1074/jbc.M611392200

Waks AG, Winer EP. 2019. Breast cancer treatment: a review. *JAMA* **321:** 288–300. doi:10.1001/jama.2018.19323

Wong YL, LeBon L, Basso AM, Kohlhaas KL, Nikkel AL, Robb HM, Donnelly-Roberts DL, Prakash J, Swensen AM, Rubinstein ND, et al. 2019. eIF2B activator prevents neurological defects caused by a chronic integrated stress response. *eLife* **8:** e42940. doi:10.7554/eLife.42940

Young AA, Bohlin HE, Pierce JR, Cottrell KA. 2024. Suppression of double-stranded RNA sensing in cancer: molecular mechanisms and therapeutic potential. *Biochem Soc Trans* **52:** 2035–2045. doi:10.1042/BST20230727

Zamanian-Daryoush M, Mogensen TH, DiDonato JA, Williams BR. 2000. NF-κB activation by double-stranded-RNA-activated protein kinase (PKR) is mediated through NF-κB-inducing kinase and IκB kinase. *Mol Cell Biol* **20:** 1278–1290. doi:10.1128/MCB.20.4.1278-1290.2000

Zhu A, Ibrahim JG, Love MI. 2019. Heavy-tailed prior distributions for sequence count data: removing the noise and preserving large differences. *Bioinformatics* **35:** 2084–2092. doi:/10.1093/bioinformatics/bty895

Zou T, Zhou M, Gupta A, Zhuang P, Fishbein AR, Wei HY, Capcha-Rodriguez D, Zhang Z, Cherniack AD, Meyerson M. 2024. *XRN1* deletion induces PKR-dependent cell lethality in interferon-activated cancer cells. *Cell Rep* **43:** 113600. doi:10.1016/j.celrep.2023.113600

MEET THE FIRST AUTHOR

Addison A. Young

***Meet the First Author(s)* is an editorial feature within *RNA*, in which the first author(s) of research-based papers in each issue have the opportunity to introduce themselves and their work to readers of *RNA* and the RNA research community. Addison A. Young is the first author of this paper, "PACT suppresses PKR activation through dsRNA binding and dimerization, and is a therapeutic target for triple-negative breast cancer." Addison A. Young is a third-year graduate student in the laboratory of Dr. Kyle Cottrell in the Department of Biochemistry at Purdue University. The Cottrell lab focuses on dsRNA binding proteins, specifically looking at the roles they play in cancer and how we can target them therapeutically. His research is primarily focused on PKR regulation in triple-negative breast cancer.**

What are the major results described in your paper, and how do they impact this branch of the field?

In this paper, we identify PACT as a suppressor of dsRNA sensing by PKR. This function is vital for the viability of triple-negative breast cancer cells. We show that depletion of PACT causes activation of the integrated stress response and NF-κB through activation of PKR, reducing cell viability. We also show that suppression of PKR activation by PACT is dependent on PACT binding dsRNA and dimerization. These findings establish PACT as a therapeutic target for the most aggressive form of breast cancer, triple-negative breast cancer.

What led you to study RNA or this aspect of RNA science?

During my undergraduate career, most of my interest in biochemistry revolved around protein structure, but as I approached graduate school my interest shifted toward RNA. From a newcomer's perspective, RNA seems functionally limited compared to protein, as RNA is both bulkier and has less diverse subunits. Yet, RNA is incredibly interesting, likely making the first enzymes and currently playing several unique roles, many of which are still undiscovered. I began to focus on dsRNAs and RNA modifications when working with Dr. Cottrell, where I officially adopted the PACT project. Working with dsRNA binding proteins has been especially interesting. I had a preconceived notion that dsRNA was only ever in the cytoplasm due to viral infection. I now understand that dsRNAs have much more diverse roles, and the idea that my work can help provide an additional glimpse into their full purpose is inspiring. Additionally, by working with breast cancer, I have had the opportunity to meet several breast cancer advocates working in Indiana trying to improve legislature for both patients and scientists. I hope that going forward I can continue to be inspired by the incredible people around me.

During the course of these experiments, were there any surprising results or particular difficulties that altered your thinking and subsequent focus?

One of our biggest struggles was immunoblotting for phosphorylated eIF2α. PKR is one of four eIF2α kinases, but we were not seeing an increase in phosphorylated eIF2α in our immunoblots when PKR was activated. At the time, we were content in showing ATF4 and NF-κB signaling downstream from PKR, which we had identified in initial RNA sequencing. I was attending a seminar where the speaker briefly mentioned that GCN2 phosphorylated eIF2α, resulting in selective translation of ATF4, increasing GADD34 levels.

Continued

GADD34 acts as a feedback regulator, dephosphorylating eIF2α when upregulated. GADD34 was not on our radar at the time, but we see a significant increase in GADD34 mRNA and protein upon PACT knockout. The high expression of GADD34 is likely dephosphorylating eIF2α, which could explain why we do not see a significant increase in phosphorylated eIF2α.

What are some of the landmark moments that provoked your interest in science or your development as a scientist?

I think the most significant part of my development as a scientist occurred during the COVID-19 pandemic. COVID-19 was the source of a lot of science-related academic momentum that could be felt even at the undergraduate level. While the challenges of being on campus were immense, I developed a strong background in both viral biology and COVID-19 itself through my coursework. This knowledge forced me to learn how to communicate these insights with my friends and my family, who often did not share my educational background. I think having this scientific background on a topic that was affecting the people I know is part of why I pursued graduate school, and I hope to be able to convey my future discoveries not just to scientific communities but also to a broader audience.

Are there specific individuals or groups who have influenced your philosophy or approach to science?

I must thank Dr. Cottrell. He is a brilliant scientist who is well versed in a variety of fields beyond what we specialize in. His presence in the lab means that we always have someone to fall back on if something goes wrong, and I could not be happier than having him as my PI. I must also thank Holly and Jackson. They were the only senior members of the lab when I joined, and their help allowed me to keep my footing when I first started. Lastly, I want to thank Dr. Steven McKenzie, my undergraduate mentor. He first helped me learn how to operate in a lab during undergrad, before helping me after graduation by teaching me how to balance graduate school with personal life.

PACT suppresses PKR activation through dsRNA binding and dimerization, and is a therapeutic target for triple-negative breast cancer

Addison A. Young, Isabelle G. Juhler, Jackson R. Pierce, et al.

RNA 2025 31: 1599-1618 originally published online August 13, 2025
Access the most recent version at doi:10.1261/rna.080637.125